



53 **INTRODUCTION**

54 The defining feature of the chordate body plan is the notochord, a principal structure formed by the axial or  
55 chorda mesoderm that provides stability and rigidity along the body axis<sup>1,2</sup>. As mammals form an ossified  
56 spine, their notochord progressively regresses and its remnants form the nucleus pulposus within the  
57 intervertebral discs<sup>3–7</sup>. Notochord precursors emerge from the initial organizer and form in a stereotypical  
58 rostral-to-caudal trajectory as gastrulation proceeds, manifesting among the earliest visible structures in  
59 chordate embryos<sup>1,8</sup>. The deeply conserved T-box transcription factor gene *Brachyury* (also called *T* or  
60 *TBX5*) is a key regulator of notochord formation. Originally identified as dominant mutation *T* that caused  
61 short tails in mice, *Brachyury* expression and function has been linked to notochord emergence across  
62 chordates<sup>9–15</sup>. In addition to its central role in notochord fate specification, the function of vertebrate  
63 *Brachyury* is required for proper primitive streak formation, tailbud specification, and subsequent  
64 neuromesodermal progenitor control<sup>16–18</sup>. However, how the expression of this central developmental  
65 transcription factor is selectively regulated to achieve its notochord activity in mammals remains unresolved.  
66

67 The central contribution of the notochord and the tailbud to different morphological adaptions and  
68 locomotion strategies shows in the diversification of axial structures across vertebrates<sup>19</sup>. Gain and loss of  
69 gene copies and of their associated gene-regulatory elements are major drivers of evolutionary innovation,  
70 and the *Brachyury* gene family itself is a prime example of this process. *Brachyury* predates the origin of, and  
71 was present as, a single copy gene in the chordate ancestor<sup>20,21</sup>. Following two whole genome duplications  
72 in early vertebrates and the subsequent loss of one of four *Brachyury* paralogs, three gene paralogs were  
73 present in the jawed vertebrate ancestor: *Tbx5a*, *Tbx5b*, and *Tbx19*<sup>21</sup>. *Tbx5a* became subsequently lost within  
74 the tetrapod lineage, resulting in mammals and birds ultimately only retaining *Tbx5b* (commonly called  
75 *Brachyury/T/TBX5* in tetrapods including humans)<sup>22</sup>. In contrast, ray-finned fishes retained both *tbx5a/ntla*  
76 and *tbx5b/ntlb*, the latter being the ortholog of the remaining human *Brachyury/T/TBX5* (*de facto TBX5*)  
77 gene<sup>17</sup>.

78 Curiously, *tbx5a/ntla* has become the predominant functional *Brachyury/T/TBX5* gene in zebrafish, as  
79 documented in classic mutants for *ntla* (*no tail a*) that fail to form a tail and notochord<sup>13,15</sup>. While no mutant  
80 for zebrafish *tbx5b/ntlb* has been reported to date, morpholino-based knockdown studies indicate that *tbx5b*  
81 function adds minimally to the dominant role of zebrafish *tbx5a*<sup>17</sup>. This variable copy number of *Brachyury*  
82 genes across vertebrates came along with selection and divergence of regulatory elements controlling  
83 *Brachyury* gene expression during distinct developmental timepoints and cell types. Promoter-proximal  
84 regions of *Brachyury* in the *Ciona* *Brachyury* gene and in the zebrafish *tbx5a* gene drive early organizer and  
85 notochord activity<sup>10,23</sup>. In contrast, the promoter-proximal region called *Tstreak* of *Brachyury/T/Tbx5b* in  
86 mouse, human, and *Xenopus* has previously been found to drive primitive streak expression in response to  
87 canonical Wnt/beta-catenin signaling, yet lacks any notochord-driving activity<sup>24–26</sup>. Further, recent work  
88 documented that deleting a large 37 kb-spanning region upstream of mouse *Brachyury/T/Tbx5b* leads to  
89 mutant phenotypes consistent with a selective loss of *Brachyury* notochord expression<sup>27</sup>. A small element  
90 termed *TNE* in the 37 kb interval was sufficient to drive specific notochord expression in mouse reporter  
91 assays, yet its deletion showed mild to no phenotypic consequences<sup>27</sup>. These pioneering data show that  
92 additional regulatory element(s) in addition to *Tstreak* and *TNE* contribute to *Brachyury/Tbx5b* expression  
93 specifically in the notochord. Uncovering the regulation of the vertebrate *Brachyury* notochord enhancer(s)  
94 will expand our understanding of the evolutionary history of this key developmental regulator and of the  
95 mechanisms leading to notochord formation. In particular, comparison to the *Ciona* *Brachyury* locus  
96 containing two upstream shadow enhancers with well-defined regulatory grammar<sup>28,29</sup> may inform *cis*-  
97 regulatory adaptations at the onset of vertebrate emergence.  
98

99 Uncovering the regulatory elements responsible for its notochord expression also promises to shed light  
100 onto the role of *Brachyury* in adult human spine health and in chordoma tumors, a rare sarcoma of the spine  
101 that is hypothesized to arise from notochord remnants<sup>30–32</sup>. Several familial chordomas harbor duplications  
102 or further complex amplifications of the *Brachyury/T/TBX5* locus that possibly convey chordoma  
103 susceptibility to carriers<sup>33–35</sup>. These findings suggest that chordoma-associated *Brachyury/T/TBX5* locus  
104 amplifications contain, or hijack the action of, *cis*-regulatory elements to possibly drive *Brachyury/T/TBX5*  
105 expression in chordoma, potentially with *Brachyury* controlling its own expression as suggested by ChIP-seq  
106 findings<sup>36</sup>.

107 Here, we identify the complement of three auto-regulated shadow enhancers *T3*, *C*, and *I* in the  
108 *Brachyury/T/Tbx5b* locus that convey notochord activity. We combined i) genomic data from human chordoma  
109 tumor cell lines, human embryonic stem cells, and mouse embryonic stem cells; ii) non-coding element

112 conservation across mammals (human, mouse, *Monodelphis*) and all vertebrates; iii) transgenic reporter  
113 assays in zebrafish, mouse, axolotl, and *Ciona*; iv) and enhancer knockouts in mice. In triple enhancer  
114 knockout mice, we document the selective absence of *Brachyury* protein in the notochord and subsequent  
115 neural tube and trunk defects as linked to notochord perturbations. Using comparative genomics, we uncover  
116 that the location and activity of the enhancers *T3*, *C*, and *I* is conserved within the *Brachyury/tbx1b* loci across  
117 jawed vertebrates. Our data uncover a deep conservation of shadow enhancers regulating *Brachyury*  
118 expression in the notochord, one of the most prominent developmental structures of the vertebrate body and  
119 involved in spine and neural tube defects.

## 122 RESULTS

### 123 Defining a region for human *Brachyury* notochord expression

124 To identify enhancer elements with notochord activity in the human *Brachyury/T/TBXTB* locus, we analyzed  
125 the *Brachyury/T/TBXTB* locus to narrow down a minimally required genomic region around the *Brachyury*  
126 gene body. Familial and sporadic chordoma feature duplications and/or complex amplifications of  
127 *Brachyury*<sup>33,34,37,38</sup>, suggesting that essential *cis*-regulatory elements for notochord expression lie within the  
128 commonly amplified region. Available genomic patient data outlined a minimally amplified region of  
129 approximately 50 kb surrounding the human *Brachyury* gene body, with individual tumors extending their  
130 amplifications proximal or distal of this minimal region<sup>34,39</sup> (Fig. 1A). Within this minimal interval and its  
131 vicinity, we uncovered several regions that have been charted as open chromatin in the chordoma cell lines  
132 U-CH2 and MUGCHOR using ATAC-seq<sup>40,41</sup>, indicating potential regulatory elements in accessible  
133 chromatin, including a super-enhancer region previously proposed to be active in chordoma<sup>40</sup> (Fig. 1A).  
134 Further, mammalian *Brachyury* has been postulated to control its own notochord expression<sup>27,42</sup>. Using  
135 *Brachyury/T* ChIP-seq data from the human chordoma tumor cell line U-CH1 and human ES-derived  
136 mesoderm progenitor cells<sup>41,43</sup>, we found discrete *Brachyury* binding events within the minimal amplification  
137 interval and its vicinity (Fig. 1A). Genome alignment of human versus other mammalian species indicated  
138 candidate enhancer regions (conserved non-coding elements; CNEs) through non-coding sequence  
139 conservation in mouse and the more distant marsupial *Monodelphis domestica*<sup>44</sup> (Fig. 1A).

140 From our combined locus analysis, we identified the six initial candidates *T3*, *K*, *J*, *C*, *I*, and *L* as putative  
141 notochord enhancer elements in the vicinity of the human *Brachyury* gene (Fig. 1A, Supplementary Data 1;  
142 all Supplementary Data is included in the Supplementary Information file). While *K* and *J* represent conserved  
143 sequence to other mammalian genomes, candidates *I* and *L* notably lie in the annotated chordoma super-  
144 enhancer region<sup>40</sup>. From this combined analysis, we hypothesized that individual or combined elements  
145 among the six enhancer candidates could convey notochord activity to the human *Brachyury* gene.

### 146 Brachyury enhancers have autonomous notochord activity

147 Given the evolutionarily conserved notochord expression of vertebrate *Brachyury* genes, we hypothesized  
148 that the human enhancers may be correctly interpreted in a model vertebrate. We initially tested all six  
149 enhancer candidates in zebrafish that allows for highly efficient reporter gene activity screening in developing  
150 embryos. To test their activity within a broad evolutionary framework, we cloned the human enhancer element  
151 candidates *T3*, *K*, *J*, *C*, *I*, and *L* into reporter vectors coupled with the mouse *betaE-globin* minimal promoter  
152 to express the blue fluorophore *mCerulean* for enhancer testing in zebrafish embryos<sup>45</sup>. Upon co-injection  
153 into one cell-stage zebrafish embryos together with *ubi:mCherry* as injection control, the human *hs\_T3*, *hs\_C*,  
154 and *hs\_I* elements resulted in *mCerulean* expression in the developing zebrafish notochord during early  
155 somitogenesis, followed by strong, selective notochord activity in injected embryos at 24 hours post-  
156 fertilization (hpf) (n=32/61, n=155/227, n=76/117; *mCerulean*-positive notochord/total *mCherry*-positive  
157 embryos) (Fig. 1B-D, Supplementary Data 2). Zebrafish embryos injected with *hs\_T3*, *hs\_C*, and *hs\_I*  
158 reporters maintained notochord-specific *mCerulean* expression throughout our observations until 5 days  
159 post-fertilization (dpf). In contrast, we did not observe any specific *mCerulean* reporter expression at any  
160 timepoint with elements *hs\_K*, *hs\_J*, and *hs\_L* (n= 0/68, n=0/63, n=0/254) (Supplementary Data 2). Notably,  
161 *hs\_C* was still active when further trimming the sequence 5' and 3' (*hs\_Cshort*, n=55/103) (Supplementary  
162 Fig. 1A-C, Supplementary Data 2). Germline-transmitted, stable transgenic integrations for *mCerulean*  
163 reporters based on *hs\_T3*, *hs\_C*, and *hs\_I* recapitulated the transient reporter results and consistently  
164 showed selective notochord expression, with minimal variability across independent transgenic insertions for  
165 each enhancer reporter (followed to at least F3 generation) (Fig. 1E-G). Together, these data indicate that  
166 the three enhancer elements *hs\_T3*, *hs\_C*, and *hs\_I* within the human *Brachyury/T/TBXTB* locus convey  
167 notochord activity when tested in zebrafish.

168 Next, we tested the activity of *hs\_T3*, *hs\_C*, and *hs\_I* in axolotl (*Ambystoma mexicanum*) as a representative  
169

172 amphibian species<sup>46,47</sup>. Upon microinjection, reporters based on *hs\_T3*, *hs\_C*, and *hs\_I* enhancer elements  
173 showed consistent reporter expression in the notochord of axolotl embryos (n=23/47, n=14/16, n=3/3)  
174 throughout tailbud stages (st. 30-41) and beyond (Fig. 1H-J, Supplementary Fig. 1D-M, Supplementary  
175 Data 2). Notably, 50% of *hs\_T3*-positive F0 animals had additional expression in other mesodermal tissues  
176 such as trunk muscles. In contrast, 80% and 100% of positive *hs\_C* and *hs\_I* F0 animals, respectively,  
177 showed expression exclusively in the notochord. In addition, *hs\_C* and *hs\_I* reporter expression was  
178 distributed along the entire rostral-caudal axis in all observed embryos, while *hs\_T3* reporter expression was  
179 frequently restricted to more caudal portions of the notochord. Combined, these results indicate that the  
180 human enhancers *hs\_T3*, *hs\_C*, and *hs\_I* also integrate regulatory input for driving notochord activity in  
181 amphibians.

182 We next tested if human enhancers *hs\_T3*, *hs\_C* and *hs\_I* also drive notochord-specific reporter activity in  
183 mouse embryos. For increased specificity and reproducibility, we used a site-directed transgenic integration  
184 strategy at the *H11* locus (enSERT)<sup>48</sup> to generate mouse embryos harboring *enhancer-LacZ* reporter  
185 transgenes. As observed in zebrafish and axolotl, *hs\_T3*, *hs\_C* and *hs\_I* elements exhibited specific and  
186 selective notochord expression in mouse embryos at E9.5 (n=3/3, n=2/2 and n=5/5) (Fig. 1 K,M,O,  
187 Supplementary Data 2). Of note, *hs\_T3* reporter activity appeared predominantly confined to the posterior  
188 notochord compared to *hs\_C* or *hs\_I*, which showed reporter activity in the entire mouse notochord.  
189 Histological analysis of Nuclear Fast Red-stained transversal sections from transgenic mouse embryos  
190 further confirmed reproducible, notochord-specific activity for human notochord enhancer elements *hs\_T3*,  
191 *hs\_C*, and *hs\_I* (Fig. 1 L, N, P).

192 Taken together, we identified three enhancer candidates in the human *Brachyury/T/TBXTB* locus, that all  
193 display notochord enhancer activity as transgenic reporters when tested in teleost fish, amphibian, and rodent  
194 embryos, suggesting pan-bony vertebrate activity and function.

### 195 **Dependence of human *Brachyury* enhancers on T-box motifs**

196 Published ChIP-seq data indicated *Brachyury* binding at *hs\_T3*, *hs\_C*, and *hs\_I* (Fig. 1A), suggesting that  
197 notochord expression of the *Brachyury/T/Tbx1b* gene might be auto-regulated by *Brachyury* itself<sup>27,42</sup>. We  
198 investigated if the three human notochord enhancer elements contained a TBXT binding motif (short T-box,  
199 Fig. 2A) using FIMO<sup>49</sup>. We found that enhancer element *hs\_T3* contained two low p-value T-box motifs,  
200 enhancer element *hs\_I* contained one low p-value T-box motif, whereas enhancer element *hs\_C* contained  
201 two possibly degenerate T-box motifs that we only identified when significantly increasing the p-value (Fig.  
202 2B), with two additional T-box motifs with even higher p-values that we did not further pursue in this work  
203 (Supplementary Fig. 2A,B). We then generated the reporter constructs *hs\_T3ΔTbox:mApple*,  
204 *hs\_CshortΔTbox:mApple*, and *hs\_IΔTbox:mApple* in which we deleted the respective T-box motifs in the  
205 enhancer elements, as well as constructs containing the wildtype enhancer elements in an identical backbone  
206 (Fig. 2C). The reporter constructs further harbored the transgenesis marker *exorh:EGFP* (expression in the  
207 pineal gland, Fig. 2D-I) for precise quantification of reporter activity<sup>45</sup>. After injection into zebrafish embryos  
208 and in line with the enhancer element activity at 24 hpf (Fig. 1B-D), we observed continued and reproducible  
209 notochord expression at 48 hpf with all three wildtype enhancer element reporters *hs\_T3:mApple*,  
210 *hs\_C:mApple*, and *hs\_I:mApple* (n=42/58, n=39/57 and n=62/79; mCerulean-positive notochord/total EGFP  
211 pineal gland-positive embryos) (Fig. 2D,F,H, Supplementary Data 2). However, we observed a complete  
212 loss of specific notochord reporter activity in zebrafish embryos injected with the deletion constructs  
213 *hs\_T3ΔTbox:mApple*, *hs\_CshortΔTbox:mApple*, and *hs\_IΔTbox:mApple* (n=6/113, n=7/53, n=1/41), with  
214 positive embryos containing few labelled notochord cells (Fig. 2E,G,I, Supplementary Data 2). In contrast,  
215 individual deletion of the high p-value T-box motifs in enhancer element *hs\_C* did not result in significant loss  
216 of reporter activity (n=28/50, n=15/63, Supplementary Fig. 2C,D).

217 Together, we conclude that the T-box motifs in the notochord enhancers *hs\_T3*, *hs\_C*, and *hs\_I* are critical  
218 to the activity of these regulatory elements in our reporter assays. These data support the model in which  
219 *Brachyury/T/TBXTB* auto-regulates its own expression in the notochord through a defined motif in its  
220 notochord regulatory elements<sup>27,42</sup>.

### 221 ***Brachyury* notochord enhancers are conserved across mammals**

222 We next sought to determine if other mammalian genomes harbor orthologous *T3*, *C*, and *I* enhancer  
223 regions in their *Brachyury/T/Tbx1b* loci. Here, we focused on the orthologous *T3*, *C*, and *I* enhancer candidate  
224 regions from mouse (Fig. 3A). As in the human *Brachyury/T/TBXTB* locus, we found open chromatin and  
225 *Brachyury* protein binding events at the mouse orthologs of the putative enhancer elements *T3*, *C*, and *I*, as  
226 well as the well-characterized murine *Brachyury/T/Tbx1b* promoter *Tstreak* (Fig. 3A).

232  
233 When transiently tested in zebrafish, both mouse enhancer *mm\_T3* and *mm\_I* showed reporter activity  
234 emerging arbitrarily throughout the gastrulating embryo at around 6 hpf (50% epiboly, shield stage)  
235 (**Supplementary Fig. 3A-D**), before expression became restricted to the developing notochord (n=46/67,  
236 n=61/66) at 24 hpf (**Fig. 3B,D, Supplementary Data 2**). Of note, our mouse enhancer *mm\_T3* contains the  
237 previously identified element *TNE*, which has been established to act as autonomous notochord enhancer  
238 when tested in mouse embryos and gastruloid cultures<sup>27</sup>. In contrast, mouse enhancer *mm\_C* failed to drive  
239 any reporter expression in the zebrafish notochord (n=0/88) (**Fig. 3C, Supplementary Data 2**). Imaging  
240 transgenic zebrafish carrying mouse *mm\_I* as stable reporter documented robust notochord expression,  
241 again with little variability across independent transgenic insertions (**Supplementary Fig. 3E**). In contrast,  
242 the murine *Brachyury/T/Tbx1b* promoter region *Tstreak*<sup>24-26</sup> showed transient, variable reporter expression  
243 in the zebrafish shield at around 6 hpf, with no reporter activity upon somitogenesis (n=79/102)  
244 (**Supplementary Data 2**). We further tested the mouse ortholog of enhancer candidate *mm\_J*, as well as the  
245 two lesser conserved elements *mm\_T1* and *mm\_T5*, none of which showed reporter activity in zebrafish  
246 embryos up to 5 dpf (n=0/98, n=0/98, n=0/79) (**Supplementary Data 2**).  
247

248 Tested with site-directed reporter transgenesis at *H11*, *mm\_T3* and *mm\_I* conveyed specific notochord  
249 activity in mouse embryos at E9.5 (n=2/2, n=4/4) (**Fig. 3E,G, Supplementary Data 2**). In contrast, and  
250 consistent with our observations in zebrafish reporter assays, *mm\_C* did not show any detectable reporter  
251 activity in the notochord in mouse embryos at E9.5 (n=0/2) (**Fig. 3F, Supplementary Data 2**).  
252

253 While humans and mice diverged approximately 90 million years ago, marsupials split from eutherians  
254 (placental mammals) approximately 160 million years ago<sup>44,50-53</sup>. The opossum *Monodelphis domestica* is a  
255 representative marsupial species and provides a more distant comparative species to human and mouse  
256 (**Supplementary Fig. 4A**). Detailed sequence alignments documented dispersed conserved regions along  
257 the entire sequences for all three enhancer candidates in *Monodelphis* (**Fig. 4A**). When injected into zebrafish  
258 embryos as *mCerulean* reporters, the *Monodelphis*-derived *md\_T3*, *md\_C*, and *md\_I* enhancer element  
259 candidates all conveyed specific notochord activity at 24 hpf (n=47/62, n=142/184, n=74/97) (**Fig. 4B-D,**  
260 **Supplementary Data 2**). Similar to the mouse elements, *md\_T3* transiently started reporter expression at  
261 around 6 hpf (**Supplementary Fig. 4B,C**), whereas *md\_C* and *md\_I* started to be active at early  
262 somitogenesis, similar to the human ones. In addition to the notochord activity, *md\_C* reporter-injected  
263 zebrafish embryos showed transient reporter expression in the heart whereas *md\_I* reporter-injected  
264 embryos showed transient expression in the brain and spinal cord neurons (**Fig. 4C,D**).  
265

266 Given the mammalian sequence conservation and differential responses in reporter assays, we next tested  
267 the notochord enhancer element candidates in the tunicate *Ciona intestinalis* as non-vertebrate outgroup. As  
268 a chordate, *Ciona* forms a bona fide notochord<sup>54</sup>. Testing *T3*, *C*, and *I* of human, mouse, and *Monodelphis*  
269 by reporter gene assays in *Ciona*, we found that only *Monodelphis*-derived *md\_C* showed specific and robust  
270 reporter activity in the notochord (n=119/150) compared to all other eight elements (n=0/150) and minimal  
271 promoter only control (n=0/150) (**Fig. 4E,F, Supplementary Data 2**).  
272

273 Taken together, and extending previous work on the mouse *TNE* element<sup>27</sup>, our data indicate that three  
274 distant elements in the mammalian *Brachyury/T/Tbx1b* locus with differential activity converge on providing  
275 notochord-specific activity in reporter assays across chordates.  
276

## 277 **Enhancer deletions cause selective loss of *Brachyury* in mice**

278 While especially enhancer element *C* seems to have diverged in activity (or is sensitive to the specific *trans*  
279 environment it was tested in), all three elements *T3*, *C*, and *I* remain conserved and detectable at the  
280 sequence level throughout the mammalian clade. In mice, homozygous *Brachyury/T/Tbx1b* mutations in the  
281 gene body cause post-implantation defects leading to embryonic lethality between E9.5 and E10.5<sup>55-57</sup>.  
282 Previous work established that deletion of mouse enhancer *TNE* does not cause a fully penetrant loss of  
283 *Brachyury/T/Tbx1b* expression in the developing notochord, indicating the presence of additional shadow  
284 elements interacting with, or compensating for, *TNE*<sup>27</sup>. To functionally test if the three enhancer elements  
285 are involved in *Brachyury/T/Tbx1b* expression in the mouse notochord, we generated a series of knockout  
286 alleles targeting the three mouse enhancer elements *T3*, *C*, and *I* (**Fig. 5A**).  
287

288 We employed CRISPR-Cas9 genome editing using target sites flanking the enhancers and established  
289 heterozygous and homozygous mice carrying individual and combined enhancer deletions (**Fig. 5A,**  
290 **Supplementary Fig. 5A**). Compared to E9.5 wildtype control embryos (**Fig. 5B**) (n=14/14), neither

292 homozygous deletion of mouse *C* ( $T^{\Delta C/\Delta C}$ ) (n=7/7) or *I* ( $T^{\Delta I/\Delta I}$ ) (n=7/7) alone, nor heterozygous ( $T^{+/+C,I}$ ) (n=12/12), heterozygous ( $T^{+/+T3}$ ) (n=7/7) (**Supplementary Fig. 5B-F**) or homozygous deletion of both *C* and *I* ( $T^{\Delta C,/\Delta C,I}$ ) (n=9/9) (**Fig. 5C**) altered *Brachyury/T/Tbx1b* expression in the notochord as determined by Brachyury/T antibody staining.

297 In contrast, we observed reduced Brachyury/T/Tbx1b expression in the notochord of E9.5 embryos in a  
298 dose-dependent manner when we combined  $\Delta T3$  with  $\Delta C,I$  deletions. E9.5 embryos heterozygous for the  
299 triple knockout chromosome carrying  $\Delta T3,C,I$  ( $T^{+/+T3,C,I}$ ) in *cis* appeared normal (n=14/14) (**Supplementary**  
300 **Fig. 5F**). In contrast, in trans-heterozygous E9.5 embryos carrying  $\Delta C,I$  and  $\Delta T3,C,I$  alleles ( $T^{\Delta C,/\Delta T3,C,I}$ ), we  
301 documented reduced Brachyury/T/Tbx1b protein in the caudal portion of the notochord in all embryos  
302 (n=18/18) with individual embryos also displaying reduced or lost Brachyury/T/Tbx1b protein in the trunk and  
303 rostral portion (n=6/18) (**Fig. 5D**). Similarly, in E9.5 embryos homozygous for  $\Delta T3$  ( $T^{\Delta T3/\Delta T3}$ ) (n=5/5) (**Fig. 5E**),  
304 we observed reduced Brachyury/T/Tbx1b protein levels, as previously reported for homozygous *TNE*  
305 embryos<sup>27</sup>. Brachyury/T/Tbx1b protein levels were even further reduced or lost in the entire notochord of  
306 trans-heterozygous for  $\Delta T3$  and  $\Delta T3,C,I$  alleles ( $T^{\Delta T3/\Delta T3,C,I}$ ) (n=10/10) (**Fig. 5F**). These data are consistent  
307 with, and expand upon, previous observations that the severity of *Brachyury/T/Tbx1b* phenotypes correlate  
308 with gene dosage<sup>57</sup>. Importantly, the  $T^{\Delta T3/\Delta T3,C,I}$  genotype with severely reduced Brachyury/T/Tbx1b protein  
309 levels is consistent with the loss of Brachyury/T/Tbx1b protein in the notochord in mice trans-heterozygous  
310 for the *TNE* deletion and a large, locus-spanning *Brachyury/T/Tbx1b* deletion that includes elements *C* and  
311 *I*<sup>27</sup>, revealing the actual relevant enhancer regions (**Fig. 1,3,4**) and motifs (**Fig. 2**). Finally, E9.5 homozygous  
312 triple knockout  $\Delta T3,C,I$  embryos ( $T^{\Delta T3,C,/\Delta T3,C,I}$ ) showed a complete absence of Brachyury/T/Tbx1b protein in  
313 the entire notochord region (n=5/5) yet all embryos retained Brachyury/T/Tbx1b protein in the tailbud (n=5/5)  
314 (**Fig. 5G**). Taken together, our data establish the notochord-specific *Brachyury/T/Tbx1b* loss-of-function  
315 mutant in mice by means of deleting three conserved enhancer elements in *cis*.

316 Next, we examined phenotypic defects resulting from perturbed *Brachyury/T/Tbx1b* expression using  
317 various allele combinations involving  $\Delta C,I$  and  $\Delta T3,C,I$ . Consistent with the phenotypes at E9.5 (**Fig. 5B-G**),  
318 we observed a gradual increase of phenotype severity with deletion of the three different enhancer elements  
319 at E12.5 (**Fig. 5H-E'**). Wildtype control (n=25/25) (**Fig. 5H,N**), homozygous  $T^{\Delta C,/\Delta C,I}$  embryos (n=24/24) (**Fig.**  
320 **5I,O**), heterozygous  $T^{+/+C,I}$  (n=5/5), heterozygous  $T^{+/+T3}$  (n=23/23) and  $T^{+/+T3,C,I}$  embryos (n=23/23)  
321 (**Supplementary Fig. 5G-I**) appeared grossly normal. In contrast, we observed rudimentary tails with  
322 additional enhancer deletions. Rudimentary tails appeared in trans-heterozygous  $T^{\Delta C,/\Delta T3,C,I}$  embryos in 4.7  
323 % (n=2/43) (**Fig. 5J,P**) and were fully penetrant in homozygous  $T^{\Delta T3/\Delta T3}$  (n=12/12) (**Fig. 5K,Q**) similar to  
324 homozygous *TNE* embryos<sup>27</sup>, and trans-heterozygous  $T^{\Delta T3/\Delta T3,C,I}$  embryos (n=14/14) (**Fig. 5L,R**), as well as  
325 in triple homozygous  $T^{\Delta T3,C,/\Delta T3,C,I}$  embryos (n=18/18) (**Fig. 5M,S**). In addition, homozygous  $T^{\Delta T3/\Delta T3}$  embryos  
326 (n=11/12) (**Fig. 5Q**) seemed to display defects in neural tube closure very close to the tail, comparable to  
327 spina bifida; upon sectioning however, we identified this region to be very small and not a fully developed  
328 spina bifida phenotype (**Fig. 5Q**). In comparison, trans-heterozygous  $T^{\Delta T3/\Delta T3,C,I}$  embryos displayed caudal  
329 spina bifida with 100% penetrance (n=14/14) (**Fig. 5R**). Finally, triple-homozygous  $T^{\Delta T3,C,/\Delta T3,C,I}$  embryos  
330 lacking all three enhancers displayed spina bifida along 3/4 of the spine (n=18/18) (**Fig. 5S**), reminiscent of  
331 previous observations using *Brachyury/T/Tbx1b*-targeting RNAi in mouse embryos<sup>58,59</sup>. These results provide  
332 compelling phenotypic evidence of the impact of cumulative enhancer deletions on *Brachyury/T/Tbx1b*  
333 expression in the notochord.

334 We further validated these phenotypes with immunohistochemistry and histology. We visualized  
335 Brachyury/T/Tbx1b protein in transversal sections of E12.5 embryos together with the neural plate marker  
336 *Sox2*: compared to wildtype (**Fig. 5T**), heterozygous  $T^{+/+C,I}$ ,  $T^{+/+T3}$ ,  $T^{+/+T3,C,I}$  (**Supplementary Fig. 5J-L**) as  
337 well as homozygous  $T^{\Delta C,/\Delta C,I}$  (**Fig. 5U**) embryos that were all grossly normal, we found decreased Brachyury  
338 protein in the notochord of  $T^{\Delta C,/\Delta T3,C,I}$  (**Fig. 5V**) and  $T^{\Delta T3/\Delta T3}$  (**Fig. 5W**) embryos. Strikingly, we observed a  
339 complete absence of Brachyury protein in  $T^{\Delta T3/\Delta T3,C,I}$  embryos (**Fig. 5X**) and  $T^{\Delta T3,C,/\Delta T3,C,I}$  (**Fig. 5Y**) embryos.  
340 In contrast, *Sox2* expression was comparable in all embryos (**Fig. 5T-Y, Supplementary Fig. 5J-L**), even in  
341  $T^{\Delta T3,C,/\Delta T3,C,I}$  embryos that clearly displayed spina bifida along the entire spine (**Fig. 5Y**). Compared to wildtype  
342 embryos (**Fig. 5Z**), additional histology assessed by H&E staining confirmed wildtype-looking notochords in  
343  $T^{+/+C,I}$ ,  $T^{+/+T3}$ ,  $T^{+/+T3,C,I}$ , and homozygous  $T^{\Delta C,/\Delta C,I}$  embryos (**Supplementary Fig. 5M-O, Fig. 5A'**), smaller (in  
344 diameter) notochords in  $T^{\Delta C,/\Delta T3,C,I}$  (**Fig. 5B'**) and  $T^{\Delta T3/\Delta T3}$  (**Fig. 5C'**) embryos, and absent notochords in  
345  $T^{\Delta T3/\Delta T3,C,I}$  and  $T^{\Delta T3,C,/\Delta T3,C,I}$  embryos (**Fig. 5D'-E'**).

346 We found that the two most severe enhancer mutants are not viable as adults since we did not recover  
347 homozygous triple  $T^{\Delta T3,C,/\Delta T3,C,I}$  (n=0/59) or trans-heterozygote  $T^{\Delta T3/\Delta T3,C,I}$  (n=0/31) animals at term  
348 (**Supplementary Fig. 5P**), indicating lethality prior to or shortly after birth. In contrast, homozygous  $T^{\Delta T3/\Delta T3}$

352 animals were born, but died within 14 days after birth, with one exception where we identified one  
353 homozygous  $T^{\Delta T3/\Delta T3}$  (n=1/34) animal without a tail that survived until adulthood (**Supplementary Fig. 5P**).  
354 In contrast,  $T^{\Delta C,/\Delta T3,C,I}$  (n=46) trans-heterozygotes and homozygous  $T^{\Delta C,/\Delta C,I}$  (n=100) animals survived to  
355 adulthood (**Supplementary Fig. 5P**). Notably, a variable percentage of  $T^{\Delta C,/\Delta C,I}$ ,  $T^{\Delta C,/\Delta T3,C,I}$ , and  $T^{+/ \Delta T3}$  animals  
356 presented with kinked tails (**Supplementary Fig. 5Q**), with two  $T^{\Delta C,/\Delta T3,C,I}$  animals displaying a small tail  
357 (**Supplementary Fig. 5R**), reminiscent of hypomorphic *Brachyury/T/Tbx1b* mutants and *in vivo*  
358 *Brachyury/T/Tbx1b* knockdown by siRNA<sup>27,58-60</sup>. Taken together, our data are consistent with the correlation  
359 of *Brachyury/T/Tbx1b*-mutant phenotypes and gene dosage controlled by enhancer activity, as revealed by  
360 increasing phenotype severity with an increasing number of combined enhancer deletions in  
361 *Brachyury/T/Tbx1b*.

362  
363 In summary, our data establishes that the combined activity of the enhancers *T3*, *C*, and *I* in the mouse  
364 *Brachyury/T/Tbx1b* locus are necessary to convey notochord expression of *Brachyury/T/Tbx1b*. Upon  
365 combined loss of these enhancers, the notochord is lost.

### 366 367 ***T3, C and I are conserved among jawed vertebrates***

368 The evolutionary trajectory of chordate *Brachyury* control in the notochord remains unresolved. The  
369 notochord-regulatory elements driving *Brachyury* expression in *Ciona* are promoter-proximal<sup>8,10,61</sup>. Zebrafish  
370 *tbxta/ntla* harbors a -2.1 kb upstream notochord element containing the two smaller elements *E1* and *E2*<sup>23</sup>.  
371 In contrast, zebrafish *tbxtb* descended from the same ancestral *Brachyury* gene as the single mammalian  
372 *Tbx1b* gene. Further, while zebrafish *tbxtb* remains expressed in the notochord<sup>21,62</sup>, its regulatory elements  
373 have not been reported. Using direct sequence comparisons of mammalian *T3*, *C*, and *I* to the zebrafish  
374 genome, we did not find any sequences of significant sequence similarity (**Fig. 1A**).  
375

376 Identifying non-coding sequence conservation across vertebrate lineages, whether from human or other  
377 tetrapods to the fast-evolving teleost fishes like zebrafish, remains notoriously challenging. Species with slow  
378 rates of molecular evolution can help as “genomic bridges” to provide sequence connectivity across distant  
379 vertebrate groups<sup>63,64</sup>. The spotted gar (*Lepisosteus oculatus*) is a slowly evolving ray-finned fish that has  
380 diverged from zebrafish and other teleosts before a teleost-specific whole-genome duplication, providing a  
381 bridge species for genomic comparisons between tetrapods and teleosts<sup>63</sup>. Using BLAST searches, we found  
382 sequence similarity between human *T3*, *C*, and *I* and regions of the spotted gar *tbxtb* locus with equivalent  
383 positions relative to the gar *tbxtb* gene body compared to mammals (**Fig. 6A**). Next, we used these spotted  
384 gar *T3*, *C*, and *I* regions as BLAST queries to bridge to the genomes of zebrafish and other fish lineages  
385 (**Supplementary Data 4**). This approach uncovered candidate regions for *T3* and *I*, but not *C*, within the  
386 zebrafish *tbxtb* locus (**Fig. 6A**).  
387

388 Analogous to our tests with mammalian enhancer candidates, we cloned reporter transgenes coupled with  
389 the *betaE-globin:mCerulean* cassette using the *T3*, *C*, and *I* enhancer elements from the spotted gar *tbxtb*  
390 locus. Upon injection into zebrafish embryos, both spotted gar *lo\_T3* and *lo\_I* displayed specific and  
391 reproducible notochord reporter activity (n=39/54, n=82/122) (**Fig. 6B,D, Supplementary Data 2**). In  
392 contrast, and akin to the mouse *mm\_C* enhancer element, spotted gar element *lo\_C* did not convey any  
393 notochord reporter activity in zebrafish embryos (n=0/92) (**Fig. 6C, Supplementary Data 2**). The zebrafish-  
394 derived *dr\_T3* and *dr\_I* also showed selective notochord activity when tested in zebrafish transgenic reporter  
395 assays (n=122/160, n=81/117) (**Fig. 6E,F, Supplementary Data 2**). Further confirming our results, we found  
396 robust reporter activity in the notochord of stable transgenic zebrafish lines based on *dr\_T3* and *dr\_I* (**Fig.**  
397 **6G,H**). All fish enhancer elements started to express the *mCerulean* reporter during early somitogenesis,  
398 similar to the human elements.  
399

400 Using the three gar elements as queries, in addition to clupecephalan teleosts (e.g. zebrafish), we found  
401 *T3* and *I* also in the other two major teleost lineages elopomorphs (e.g. eel) and osteoglossomorphs (e.g.  
402 arowana). However, we did not detect any equivalent sequence for *C* in any teleosts, indicating that this  
403 element has been lost or diverged beyond recognition in the teleost lineage (**Fig. 6I**). However, we detected  
404 orthologs of all three elements, including *C*, at expected locations around the *tbxtb* genes in additional non-  
405 teleost ray-finned fishes (e.g. bowfin, sturgeon, reedfish) as well as in the more basally diverging cartilaginous  
406 fishes (e.g. sharks, skate) (**Supplementary Data 4**); in contrast, we only detected *T3* and *I* in the lobe-finned  
407 coelacanth (**Fig. 6I**). To explore the presence of the three enhancer elements among tetrapods, we used the  
408 painted turtle, characterized by a slow genomic evolutionary rate<sup>65,66</sup>, as an additional bridge species within  
409 tetrapods. We found all three elements in the turtle *Brachyury/T/Tbx1b* locus and through use of the painted  
410 turtle as reference also in other reptiles and birds, as well as in amphibians (e.g. axolotl) (**Fig. 6I**,  
411

412 **Supplementary Data 4**), but did not detect any of the three elements in the jawless cyclostome (e.g. lamprey, 413 hagfish) genomes. Furthermore, we found that the human T-box motifs, which we identified using FIMO (Fig. 414 2) in our enhancers, are conserved across tetrapods and fishes as distantly related as ghost shark based on 415 sequence alignments (**Supplementary Fig. 6A-C**) as well as multi-species FIMO analyses (**Supplementary 416 Data 7**). Cross-species sequence conservation centers at the T-box motifs (**Supplementary Fig. 6A-C**) 417 which supports both their functional importance as well as their evolutionary ancestry since at least the last 418 common ancestor of jawed vertebrates.  
419

420 Taken together, our observations provide strong evidence that notochord enhancers *T3*, *I*, and *C* are deeply 421 conserved *cis*-regulatory elements of the *Brachyury/T/Tbx1b* gene that were already present in the last 422 common ancestor of jawed vertebrates over 430 million years ago.  
423  
424

## 425 **DISCUSSION**

426 How the *Brachyury/T/Tbx1b* gene is controlled during notochord development is fundamental to our 427 understanding of how basic concepts of body plan formation remain conserved or have diverged across 428 species. Shadow enhancers, seemingly redundant transcriptional *cis*-regulatory elements that regulate the 429 same gene and drive overlapping expression patterns, are a pervasive feature of developmental gene 430 regulation<sup>67</sup>. The concept of enhancer redundancy through one or more shadow enhancers acting on the 431 same gene in addition to primary enhancer has been established for numerous loci<sup>67-72</sup>. Shadow enhancers 432 are thought to provide robustness to gene expression and buffer against genetic and environmental 433 variations<sup>67,73</sup>, a hypothesis validated in mammals<sup>71,72</sup>.  
434

435 Here, we discovered a deeply conserved set of three notochord-specific shadow enhancers within the 436 human TBXT locus as ancient *cis*-regulatory **elements**. While we cannot draw conclusions about reporter 437 initiation or early reporter expression patterns, cross-species enhancer testing reveals that the *cis*-regulatory 438 grammar of the three human enhancers *T3*, *C*, and *I*, is correctly interpreted in vertebrates including mice, 439 salamanders, and zebrafish, but not in the invertebrate chordate *Ciona*. The three notochord enhancers 440 described here are not the only non-coding conserved elements across mammalian *Brachyury/T/Tbx1b* loci 441 (**Fig. 1A, 3A, 4A**). Even though our zebrafish reporter assays did not reveal any notochord activity in three 442 out of the six tested human enhancer elements (*K*, *J*, and *L*), we cannot rule out synergistic or interdependent 443 notochord activity conveyed by additional elements. Further, our reporter assays indicate that not all three 444 *Brachyury/T/Tbx1b* notochord enhancers *T3*, *C*, and *I* have equal potency. Enhancer element *C* shows 445 variable activity and remains unrecognized in teleost fishes and Coelacanth. Compared to human *C* with 446 reproducible notochord activity in all tested models (**Fig. 1C,F,I,M**) and *Monodelphis C* that is active in 447 zebrafish and uniquely in *Ciona* (**Fig. 4C,E**), mouse *C* showed no discernible activity in any assay including 448 in mouse embryos (**Fig. 3C,G**) despite significant sequence conservation. We speculate that while mouse *C* 449 is not active in isolation, it may contribute together with *T3* and *I* to *Brachyury* activity in the notochord. This 450 model is consistent with the impact of *TNE* deletions when combined with larger deletions that include *TNE* 451 and *C* in mouse trans-heterozygotes<sup>27</sup> (**Fig. 5**). The potential auto-regulation of *Brachyury/T/Tbx1b* by its 452 protein product via in part conserved T-box motifs in enhancers *T3* and *I* might contribute to the enhancer 453 redundancy and divergent activity of element *C* when tested in isolation (**Fig. 2**). Our data propose that 454 enhancer *C* is an auxiliary element to *T3* and might contribute to duration, expression levels, or other features 455 that differ among *Brachyury/T/Tbx1b* notochord expression across vertebrates. Our combined data proposes 456 a model in which notochord expression of vertebrate *Brachyury/T/Tbx1b* is cumulatively or cooperatively 457 driven by enhancers *T3*, *C*, and *I*. In this model, sequence variants of *T3*, *C*, and *I* that modulate their 458 individual potency became selected for modulating *Brachyury/T* levels to species-specific requirements.  
459

460 The conservation of gene order (micro-synteny) between species can be indicative of the presence of *cis*- 461 regulatory elements, which are crucial for controlling expression of the physically linked genes<sup>74</sup>. The finding 462 of functionally relevant distant enhancers 5' and 3' of the *Brachyury/T/Tbx1b* gene body is further supported 463 by the conserved gene linkage *Sftd2-(Prr18)-Brachyury/T/Tbx1b-Pde10a* across the entire jawed vertebrate 464 phylogeny. In agreement with a distinct gene linkage surrounding *Brachyury/T/Tbx1b* in agnathans (**Fig. 6I**), 465 we were unable to identify any of the three distant enhancers in two species representing this clade. Likewise, 466 a distinct gene linkage associates with *Tbx1a*, the second *Tbx1b* paralog in fish, which apparently lacks any 467 of the three notochord enhancers described here. *tbx1a/ntla* expression is instead controlled by two 468 mesoderm/notochord enhancers located close to the gene promoter (Harvey et al., 2010), a possible 469 example of evolutionary novelty following ancestral gene duplication. In contrast, the functionally less 470 impactful zebrafish *tbx1b/ntlb* gene retained the **regulation** of the *Tbx1b* gene from the jawed vertebrate 471 ancestor (**Fig. 6**). We did not find any evidence for sequence conservation of the *Tbx1b* *T3*, *I*, or *C* regions

472 within vertebrate *Tbxta* loci or any other genomic regions. Future detailed studies across vertebrate *Tbxt*  
473 paralogs are needed to evaluate whether or not the three *Tbxtb* regulatory elements identified here were  
474 already part of the single *Tbxt* gene in a vertebrate ancestor. Notably, zebrafish mutants of *tbxta/ntla* have  
475 been widely studied as model for *Brachyury* function in notochord formation<sup>13,15,75</sup>, while the seemingly less  
476 impactful *tbxtb* has retained ancestral regulation. Why zebrafish, and possibly other fish lineages, use *tbxta*  
477 as their main functional *Brachyury* paralog, and how the regulatory balance between *T3*, *C*, and *I* plays out  
478 across individual vertebrate lineages, warrants future efforts.  
479

480 We found that *Brachyury/T/Tbxtb* notochord enhancers *T3* and *I*, and possibly further supported by  
481 enhancer *C*, represent a shadow enhancer combination that contributes to the robust *Brachyury/T/Tbxt*  
482 expression in mammals. In mice, neither deletion of enhancer *T3/TNE*<sup>27</sup>, nor deletion of enhancer *C*, *I*, or *C*  
483 and *I*, resulted in a discernable notochord phenotype (Fig. 5). Nonetheless, by combining deletions of all  
484 three notochord enhancer elements, we showed a dose response for *Brachyury/T* expression in the  
485 notochord. In particular, in embryos where  $\Delta T3$  is combined with a chromosome harboring  $\Delta T3, C, I$  as trans-  
486 heterozygotes ( $T^{\Delta T3/\Delta T3, C, I}$ ) or in triple homozygous knock-out embryos ( $T^{\Delta T3, C, I/\Delta T3, C, I}$ ), we observed loss of  
487 *Brachyury/T* protein in the notochord as well as notochord-specific phenotypes, such as spina bifida (Fig. 5).  
488 The neural tube closure defects are similar to phenotypes observed in *Brachyury/T/Tbxtb* knockdown  
489 embryos<sup>58,59</sup> or hypomorphic *Brachyury/T/Tbxtb* mutants<sup>60</sup>. These results assign an essential, combinatorial  
490 role to the enhancer elements *T3/TNE*, *C* and *I* in regulating *Brachyury/T/Tbxtb* in the notochord. Notably,  
491 previous work<sup>76,77</sup> has described the *T2* mutant caused by a large viral integration 5' of the mouse  
492 *Brachyury/Tbxt* locus that i) is recessive lethal with phenotypes reminiscent of *Brachyury* loss, and ii) does  
493 complement loss-of-function alleles for *Brachyury*. *T2* has been hypothesized to encode a short protein off a  
494 long mRNA<sup>76,77</sup>. The described genomic position of the viral integration in *T2* places it in the vicinity and  
495 upstream of enhancer element *C*. We note that various vertebrate *Brachyury/tbxtb* loci feature annotated  
496 long non-coding RNAs upstream of the main gene body that are reminiscent of enhancer RNAs (Fig. 3A,  
497 6A). We therefore hypothesize that the *T2* mutation is caused by a disruption of the gene-regulatory  
498 landscape of the mouse *Brachyury/Tbxt* gene by the viral integration, changing the interaction of distant  
499 enhancer elements with the promoter. Inspection of the chromatin landscape of the *Brachyury/Tbxt* locus,  
500 also in *T2* mutants, could shed light on the architecture of the locus during notochord development.  
501

502 The significance of *Brachyury/T/Tbxtb* regulation in the notochord translates to chordoma tumors that  
503 feature expression of this T-box transcription factor as key diagnostic readout<sup>32,78,79</sup>. Both sporadic and  
504 familial chordoma are hypothesized to derive from notochord remnants in the spine that do not convert to  
505 nucleus pulposus tissue<sup>32,80,81</sup>. Native *Brachyury*-expressing cells in the nucleus pulposus decrease in  
506 number with age along with a concomitant increase in cartilage-like cells<sup>4,82–84</sup>. What role these long-lasting  
507 *Brachyury*-positive cells play in the adult spine, if they progressively differentiate into cartilage, and how  
508 *Brachyury* gene activity is sustained, remains unknown. Detection of *Brachyury* protein is a diagnostic marker  
509 for chordoma<sup>32</sup>, yet the functional contribution of its re-activated or persistent expression in the tumor remains  
510 unknown<sup>59,85–87</sup>. Our analysis of reported familial and sporadic chordoma amplifications indicate that  
511 amplifications invariantly retain the notochord enhancer *I* together with the gene body including the  
512 promoter<sup>34,37</sup>. Enhancer *I* lies within a super-enhancer region identified in chordoma cell lines<sup>40</sup>, further  
513 implicating its transcriptional engagement in chordoma. Amplifications occurring in tandem with the original  
514 locus propose a scenario where the retained enhancer *I* could synergize with *C* and *T3* from the original locus  
515 on the newly amplified gene copies, potentially resulting in increased *Brachyury/T/TBXTB* expression (Fig.  
516 1A). Beyond chordoma, changes in enhancer sequence or relative distance to the *Brachyury/T/TBXTB* gene  
517 body could also impact spine formation and health by altering the robustness of *Brachyury* expression in the  
518 notochord and subsequent nucleus pulposus.  
519

520 Tremendous progress in *in vitro* differentiation regimens have resulted in stem cell-derived models for body  
521 segmentation and different organ structures<sup>88–91</sup>. However, notochord formation has only been reported in  
522 more complex systems that recapitulate major hallmarks of embryo patterning<sup>92–94</sup>. Reporters based on our  
523 isolated enhancers could potentially provide potent readouts to screen for differentiation regimens that result  
524 in notochord fates. Together, our uncovered set of shadow enhancers in *Brachyury/T/TBXTB* advance our  
525 concepts of how this key contributor to notochord formation is regulated and de-regulated in development  
526 and disease.  
527  
528  
529  
530

531 **METHODS**

532 **Ethical regulations**

533 All research within this manuscript complies with all relevant ethical regulations that are described and named  
534 individually in each paragraph.

535 **Brachyury locus annotations**

536 The UCSC genome browser was used to identify and visualize enhancer elements in the human, mouse,  
537 and *Monodelphis* *Brachyury* locus. \*.bed files were generated with the approximate genomic location of  
538 human *Brachyury* amplifications in chordoma tumors from different patients<sup>34,37</sup>. Previously published ATAC  
539 sequencing data of U-CH2 cells and MUGCHOR cells<sup>40</sup>, as well as *Brachyury*/T ChIP sequencing data of  
540 human embryonic stem cells (hESCs)<sup>43</sup> and U-CH1 cells<sup>41</sup> were added. Further, the repeat masker track,  
541 ENCODE cCREs, layered H3K27ac, and the conservation track for mouse and *Monodelphis* were added.  
542 Ultimately, using this strategy, the human enhancer element candidates *T3*, *K*, *J*, *C*, *I*, and *L* were identified.  
543 For detailed information, see **Supplementary Data 1 and 3**.

544 The same strategy was applied to find the corresponding mouse enhancer elements. Published ATAC-seq  
545 data of mouse ESCs<sup>95</sup> and *Brachyury*/T-positive fluorescence-activated cell sorted cells from the caudal ends  
546 of wild-type mouse embryos (TS12/8 dpc and TS13/8.5 dpc)<sup>96</sup>, as well as *Brachyury*/T ChIP sequencing data  
547 of mouse ESCs<sup>42,96</sup> were used. Again, the repeat masker track, the ENCODE Candidate Cis-Regulatory  
548 Elements (cCREs, combined from all cell types) track, tracks containing H3K27ac, H3K4me, DNase signals  
549 from E11.5 neural tube as it likely contains notochord tissue as well due to extraction<sup>97</sup>, and the Vertebrate  
550 Multiz Alignment & Conservation track to check for conservation in human, *Monodelphis*, and zebrafish, were  
551 added. This approach identified the mouse enhancer element candidates *T1*, *T2*, *T3*, *J*, *C2/next to C*, *C*,  
552 *Tstreak*, *I*, *T4*, *T5*, and *T6*, of which *T1*, *T3*, *J*, *C*, *Tstreak*, *I*, and *T5* were pursued and tested (**Supplementary**  
553 **Data 3 and 5**).

554 To find the corresponding *Monodelphis* elements, the repeat masker and 9-Way Multiz Alignment &  
555 Conservation track were included to identify *T3*, *C*, and *I* (**Supplementary Data 3 and 5**).

556 **Cloning of the enhancer element reporter plasmids**

557 Each *Brachyury* enhancer element candidate was amplified from either human, mouse, *Monodelphis*,  
558 spotted gar, or zebrafish genomic DNA using the Expand Hi-Fidelity PCR System (11732641001, Roche).  
559 Exact coordinates are listed in **Supplementary Data 3**. Each enhancer candidate was TOPO-cloned into the  
560 *pENTR5'-TOPO* plasmid (K59120, Invitrogen) using half-volume reactions according to the manufacturer's  
561 instructions (half-volume reactions). Subsequent Multisite Gateway cloning (half-volume reactions) were  
562 performed using LR Clonase II Plus (12538120, Invitrogen) according to the manufacturer's instructions (half-  
563 volume reactions) and recommended reaction calculations<sup>98</sup>. 5' entry plasmids containing the different  
564 enhancer elements were assembled into reporter expression plasmids together with the middle entry plasmid  
565 (*pME*) containing the mouse *betaE-globin* minimal promoter expressing mCerulean (*pSN001*) as well as  
566 mApple (*pCK068*), the 3'plasmid #302 (*p3E\_SV40polyA*), and the destination plasmid *pDESTTo12A2*  
567 containing *crybb1:mKate2* (*pCB59*) and *pDESTtexor:EGFP* containing EGFP expression in the pineal gland  
568 (*pCK017*) as transgenesis markers<sup>45</sup>. Assembled vectors were verified using restriction digest and Sanger  
569 sequencing using standard sequencing primers for Multisite Gateway assemblies<sup>45,98</sup>.

570 **Zebrafish husbandry, transgenic reporter assays and stable transgenic lines**

571 Zebrafish animal care and procedures were carried out in accordance with the IACUC of the University of  
572 Colorado Anschutz Medical Campus (protocol # 00979), Aurora, Colorado. Adult AB and TU wildtype  
573 zebrafish were obtained from the Zebrafish International Resource Center (ZIRC) and maintained as per  
574 standard husbandry procedures<sup>99</sup>.

575 To test the transient activity of the putative enhancer elements, 25 ng/µL *To12* mRNA, 12.5 ng/µL reporter  
576 expression plasmid DNA, and 12.5 ng/µL *ubi:mCherry* plasmid<sup>100</sup> as injection control were co-injected into  
577 one-cell stage wild type zebrafish embryos<sup>47</sup>. At 24 hpf, embryos were anesthetized with 0.016% Tricaine-S  
578 (MS-222, Pentair Aquatic Ecosystems Inc.) in E3 embryo medium and embedded in E3 with 1% low-melting-  
579 point agarose (A9045, Sigma Aldrich).

580 To generate stable transgenic lines, 25 ng/µL *To12* mRNA were co-injected with 25 ng/µL reporter  
581 expression plasmid DNA<sup>101,102</sup>. Multiple F0 founders were screened for specific *mCerulean* and *mKate2*  
582 expression, raised to adulthood, and screened for germline transmission. Resulting F1 single-insertion  
583 transgenic strains were established and verified through screening for a 50% germline transmission rate  
584 outcrosses in the subsequent generations as per our previously outlined procedures<sup>102</sup>. *Tg(drl:mCherry)* was  
585 used as a marker for lateral plate mesoderm derivatives<sup>44</sup>.

590 For imaging, embryos were mounted laterally on glass bottom culture dishes (627861, Greiner Bio-One)  
591 and confocal images were acquired with a Zeiss LSM880 using a  $\times 10/0.8$  air-objective lens. Fluorescence  
592 channels were acquired sequentially with maximum speed in bidirectional mode in  $3\text{ }\mu\text{M}$  slices. The range of  
593 detection for each channel was adapted to avoid any crosstalk between the channels. Images of acquired Z-  
594 stacks were reconstructed with ImageJ/Fiji as a maximum intensity projections.

595

### 596 **Axolotl husbandry, transgenic reporter assays and immunostaining**

597 Procedures for care and manipulation of all animals used in this study were performed in compliance with  
598 the laws and regulations of the State of Saxony, Germany. Axolotl husbandry and experiments (non-free  
599 feeding stages) were performed at the Center for Regenerative Therapies Dresden (CRTD), Dresden,  
600 Germany. Adult axolotls (*Ambystoma mexicanum*) were obtained from the axolotl facility at the Technische  
601 Universität Dresden (TUD)/CRTD Center for Regenerative Therapies Dresden. Animals were maintained in  
602 individual aquaria at  $\sim 18\text{--}20\text{ }^{\circ}\text{C}$ <sup>103</sup>. Axolotls of the white (d/d) strain were used in all experiments.

603 Transgenic axolotl embryos were generated using *Tol2* transposase following standard protocols<sup>104</sup>. For  
604 live imaging, the embryos were anaesthetized by bathing in 0.01% benzocaine and imaged on an Olympus  
605 SZX16 fluorescence stereomicroscope. Embryos were staged as described previously<sup>105</sup>.

606 For immunostaining, axolotl embryos were fixed in MEMFA at  $4\text{ }^{\circ}\text{C}$  overnight, washed in PBS, embedded  
607 in 2% low-melting temperature agarose, and sectioned by vibratome into  $200\text{ }\mu\text{m}$ -thick sections. Fibronectin  
608 was detected using mouse anti-Fibronectin (ab6328, Abcam; dilution 1:400) and donkey anti-mouse Alexa  
609 Fluor™ 568 (A-10037, Invitrogen; dilution 1:600). After staining, sections were mounted with Mowiol (81381,  
610 Millipore Sigma). Confocal images were acquired on a Zeiss LSM780-FCS inverted microscope.

611

### 612 **Transgenic mouse reporter assays**

613 Research was conducted at the E.O. Lawrence Berkeley National Laboratory (LBNL) and performed under  
614 U.S. Department of Energy Contract DE-AC02-05CH11231, University of California (UC). Transgenic mouse  
615 assays were performed in *Mus musculus* FVB mice (obtained from The Jackson Laboratory), animal protocol  
616 number 290003; reviewed and approved by the Animal Welfare and Research Committee at Lawrence  
617 Berkeley National Laboratory.

618 For comprehensive analysis of species-specific *T3*, *C* and *I*, enSERT enhancer analysis was used, allowing  
619 for site-directed insertion of transgenic constructs at the *H11* safe-harbor locus<sup>106,107</sup>. EnSERT is based on  
620 co-injection of Cas9 protein and *H11*-targeted sgRNA in the pronucleus of FVB single cell-stage mouse  
621 embryos (E0.5) with the targeting vector encoding a candidate enhancer element upstream of the *Shh*-  
622 promoter-*LacZ* reporter cassette<sup>48</sup>. Enhancer elements were PCR-amplified from human, mouse and  
623 Monodelphis genomic DNA and cloned into the respective *LacZ* expression vector<sup>108</sup>. Embryos were  
624 excluded from further analysis if they did not contain a reporter transgene in tandem. CD-1 females (The  
625 Jackson Laboratory) served as pseudo-pregnant recipients for embryo transfer to produce transgenic  
626 embryos which were collected at E9.5 and stained with X-gal using standard methods<sup>108</sup>.

627

### 628 **Histological analysis of Nuclear Fast Red-stained sections from transgenic mouse embryos**

629 After LacZ staining, E9.5 transgenic mouse embryos were dehydrated in serial alcohols (1x 70%, 1x 80%,  
630 1x 90%, 2x 96%, 2x 100% ethanol, followed by 1x 100% isopropanol for 20 minutes each) and cleared twice  
631 for 30 minutes with Histo-Clear II (HS-202, National Diagnostics) for paraffin wax embedding. 10  $\mu\text{m}$ -thick  
632 transverse sections were obtained with a Leica Biosystems RM2245 Semi-Automated Rotary Microtome.  
633 Sections were de-waxed, rehydrated, and stained with Nuclear Fast Red (R5463200, Ricca Chemical) for  
634 two minutes. After staining, sections were dehydrated and mounted with Omnimount (HS-110, National  
635 Diagnostics). Images were obtained using a Leica M205 FA stereo microscope.

636

### 637 **Ciona reporter assays**

638 Ciona experiments were performed at UCSD as described previously<sup>29,109</sup>. Adult *Ciona intestinalis* type A  
639 aka *Ciona robusta* (obtained from M-Rep) were maintained under constant illumination in seawater (obtained  
640 from Reliant Aquariums) at  $18\text{ }^{\circ}\text{C}$ . Briefly, human, mouse and Monodelphis enhancer elements *T3*, *C* and *I*  
641 were subcloned into appropriate plasmids suited for expression in Ciona, upstream of a basal Ciona  
642 Forkhead promoter driving GFP<sup>28,110</sup>. Ciona embryos were electroporated with 70  $\mu\text{g}$  of each plasmid as  
643 previously described<sup>111</sup> and reporter expression was counted blind in 50 embryos per biological repeat. All  
644 constructs were electroporated in three biological replicates. Images were taken of representative embryos  
645 with an Olympus FV3000 microscope using a 40X objective.

646

### 647 **Deletion of mouse enhancer elements *T3*, *C* and *I***

648 All mouse experimental procedures and animal care were approved by the Animal Care Committee of the  
649 Institute of Molecular Genetics (IMG), Czech Academy of Sciences, Prague, Czech Republic, and covered

under protocol permission number 357/2021. Experiments were performed in compliance with the European Communities Council Directive of November 24, 1986 (86/609/EEC), as well as national and institutional guidelines.

For this study, inbred C57BL/6N mice (The Jackson Laboratory) were used. Mice carrying deletions of enhancer elements *T3*, *C*, and *I* were generated using CRISPR-Cas9 technology. The cRNAs (purchased from Integrated DNA technologies, IDT) were designed to target the 5' and 3' ends of the mouse enhancer elements *T3*, *C* and *I* to delete the genomic regions in between. For genomic location and sequence of the selected target sites, as well as genomic coordinates of the deleted enhancer element sequences, see **Supplementary Data 5**.

A ribonucleoprotein (RNP) complex of crRNA/TRACR (1072532, IDT) and SpCas9 protein (1081058, IDT) was electroporated into fertilized zygotes isolated from C57BL/6N mice. Zygote electroporation and transfer into pseudo-pregnant foster females was performed as previously described<sup>112</sup>. Founder animals from multiple embryo transfers were genotyped from tail biopsies using PCR and Sanger sequencing and the positive animals were backcrossed to C57BL/6N mice.

Independent knockout lines for enhancer element *C* ( $\Delta C$ ) and *I* ( $\Delta I$ ) were generated. Heterozygous  $\Delta C$  and  $\Delta I$  ( $T^{+\Delta C}$  and  $T^{+\Delta I}$ ) and homozygous  $\Delta C$  and  $\Delta I$  ( $T^{\Delta C/\Delta C}$  and  $T^{\Delta I/\Delta I}$ ) embryos were investigated for potential overall phenotypes, but appeared phenotypically normal. Pups were born normally and grew up into fertile adults.

To generate a double knockout  $\Delta C, \Delta I$  strain, homozygous  $T^{\Delta C/\Delta C}$  mice were used for electroporation of CRISPR-Cas9 RNP complexes deleting enhancer element *I*. Pups homozygous for  $\Delta C, \Delta I$  ( $T^{\Delta C, \Delta I/\Delta C, \Delta I}$ ) were born phenotypically normal and developed into fertile adults; however, around 20% of the animals had a kinked tail (**Supplementary Fig. 5M,N**).

To generate a triple knockout  $\Delta T3, C, I$  mouse strain, heterozygous  $\Delta C, \Delta I$  ( $T^{+\Delta C, \Delta I}$ ) mice were used for electroporation of CRISPR-Cas9 RNP complexes deleting enhancer element *T3* ( $\Delta T3$ ). Heterozygous  $T^{+\Delta T3, C, I}$  or trans-heterozygous  $T^{\Delta T3/\Delta C, I}$  embryos were phenotypically normal and grew up into fertile adults. To establish a single knockout line for enhancer element *T3* ( $\Delta T3$ ),  $T^{\Delta T3/\Delta C, I}$  animals were outcrossed to establish  $T^{+\Delta T3}$ .

$T^{\Delta C, \Delta I/\Delta T3, C, I}$  animals were generated by mating  $\Delta C, \Delta I$  ( $T^{\Delta C, \Delta I/\Delta C, \Delta I}$ ) and  $\Delta T3, C, I$  ( $T^{+\Delta T3, C, I}$ ) strains and  $T^{\Delta T3/\Delta T3, C, I}$  by mating  $\Delta T3$  ( $T^{+\Delta T3}$ ) and  $\Delta T3, C, I$  ( $T^{+\Delta T3, C, I}$ ) strains, respectively. Finally, homozygous  $T^{\Delta T3, C, I/\Delta T3, C, I}$  animals were generated by mating trans-heterozygous  $\Delta C, \Delta I/\Delta T3, C, I$  ( $T^{\Delta C, \Delta I/\Delta T3, C, I}$ ) animals.

Around 60% of  $T^{\Delta C, \Delta I/\Delta T3, C, I}$  pups were born with a tail defect and adult animals displayed a kinked tail, with around 2% of the  $T^{\Delta C, \Delta I/\Delta T3, C, I}$  pups displaying a small tail. In contrast, adult trans-heterozygous  $T^{\Delta T3/\Delta T3, C, I}$  and homozygous  $T^{\Delta T3, C, I/\Delta T3, C, I}$  animals were never recovered likely due to lethality at around birth or during early postnatal life.

The deletion breakpoints in the individual enhancer alleles were determined by Sanger sequencing. Mice were genotyped using PCR with dedicated primer sets (**Supplementary Data 5**). Mouse embryos of the given stage were harvested from timed pregnant mice. The day of plug was counted as embryonic day 0.5 (E0.5).

688

### 689 **E9.5 whole mount immunostaining and imaging**

690 E9.5 mouse embryos were collected and whole mount immunostaining was done as previously  
691 described<sup>113</sup>. Brachyury/T/Tbx5 expression in E9.5 embryos was visualized using rabbit anti-Brachyury  
692 (ab209665, Abcam; dilution 1:2000) and donkey anti-rabbit Alexa Fluor™ 594 (A-21207, Invitrogen, dilution  
693 1:500). Images were obtained using a Zeiss AxioZoom V16 microscope with Apotome with a Zeiss Axiocam  
694 512 mono camera. A qualitative analysis of all investigated embryos can be found in **Supplementary Data**  
695 **6**.

696

### 697 **E12.5 embryo preparation, immunostaining and imaging**

698 E12.5 mouse embryos were collected and fixed overnight in 4% paraformaldehyde. Whole embryo images  
699 were acquired using a Olympus SZX9 stereo microscope with a Olympus DP72 camera. Afterwards, embryos  
700 were embedded in paraffin, and 9  $\mu$ m-thick transverse sections were obtained using a Microtome Leica  
701 RM2255. Sections were deparaffinized, rehydrated, and stained with hematoxylin & eosin (H-3502,  
702 Vectorlabs) for histology, or rabbit anti-Brachyury (ab209665, Abcam; dilution 1:2000) and donkey anti-rabbit  
703 Alexa Fluor™ 594 (A-21207, Invitrogen, dilution 1:500), or goat anti-Sox2 Y-17 (sc-17320, Santa Cruz;  
704 dilution 1:400) and donkey anti-goat Alexa Fluor™ 488 (A-11055, Invitrogen, dilution 1:500) together with  
705 DAPI (10236276001, Roche Diagnostics) according to the manufacturer's instructions. After staining,  
706 sections were mounted with Mowiol (81381, Millipore Sigma). Images of sections were obtained using a Leica  
707 DM6000 widefield fluorescence microscope with a Leica DFC 9000 camera.

708

### 709 **Gar and turtle bridge alignment**

710 To establish genomic connectivity across distant vertebrate lineages, a bridging approach that leverages  
711 species with slowly evolving genomic sequences, such as spotted gar within ray-finned fishes<sup>63</sup> and painted  
712 turtle within tetrapods<sup>114</sup>, was used. Using human *T3*, *C*, and *I* as queries, BLASTN searches at  
713 ensembl.org<sup>115</sup> (search sensitivity: distant homologies) against the bridge species genomes were performed.  
714 Candidate BLAST hit regions were manually inspected for their location in relation to the *Tbx1b* gene locus  
715 for further consideration. Core regions based on the initial BLAST hits in both bridge species were expanded  
716 in both directions up to the next annotated repeat element. Once the three elements were established in the  
717 bridge species, their sequences were used for as queries for BLASTN searches with genomes representative  
718 species across all major vertebrate lineages as targets (see **Supplementary Data 4** for species list, genome  
719 assemblies, and enhancer element coordinates). Further BLASTN chaining through additional species was  
720 performed as needed (e.g., human->gar->goldfish->zebrafish for *T3* and *I*). All BLAST hits were manually  
721 inspected for proximity to the *Tbx1b* gene. Multi-species alignments of the three elements were generated  
722 with MAFFT version 1.5.0<sup>116</sup>.

## 723 **Identifying T-box motifs**

724 The presence of T-box motifs in the individual species was established with FIMO version 5.5.4<sup>117</sup> at  
725 <https://meme-suite.org/meme/tools/fimo> using as input sequence the human TBXT motif  
726 *TBXT\_MA0009.2.meme* obtained from JASPAR 2022<sup>118</sup> at <https://jaspar.genereg.net/>.

## 730 **Statistics and Reproducibility**

731 The authors declare that key measures of statistics and reproducibility are built into the work throughout.  
732 For the zebrafish, axolotl, mouse, and *Ciona* reporter assays, as well as the mouse knockout studies,  
733 sufficient embryos were analyzed to achieve statistical significance based on previous experience in  
734 transgenic reporter assays and mouse knockout studies. Experimental sample sizes were chosen by  
735 common standards in the field and in accordance with solid phenotype designation<sup>119-122</sup>. For the mouse  
736 reporter assays, sample sizes were selected empirically for >3,000 total putative enhancers (VISTA Enhancer  
737 Browser, <https://enhancer.lbl.gov/>)<sup>123</sup>.

738 All transgenic reporter assays, as well as the knockout experiments, were treated with identical  
739 experimental conditions across species and performed at least twice or more times in the majority of  
740 instances. All attempts at replication were successful.

741 No data were excluded in the zebrafish, axolotl, mouse or *Ciona* reporter assays, as well as the mouse  
742 knockout studies.

743 Data analyses of the transgenic reporter quantification was based on injections into zebrafish, axolotl, and  
744 mouse embryos/electroporation into *Ciona* embryos, and knockout quantification was based on defined  
745 genotypes of mouse embryos from crosses. No other randomizations were applicable.

746 Data collection for transgenic and knockout analyses was unblinded as it required reporter activity and  
747 phenotype assessment as well as genotyping analysis to confirm transgenic or mutant versus wildtype.

748 Zebrafish and axolotl embryos were not selected by gender as sex determination happens later in  
749 development. *Ciona* are hermaphroditic, therefore there is only one possible sex for individuals. Mouse  
750 embryos of both sexes were used in transgenic and knockout analyses and no differences in gender were  
751 observed in those experiments.

## 752 **Data Availability**

753 The authors declare that all the data supporting the findings of this study are available within the paper and  
754 its supplementary information files.

755 The genome tracks using published data are deposited in a publicly accessible repository (UCSC browser).

756 The *hg38* UCSC browser session can be found here: [https://genome.ucsc.edu/cgi-bin/hgTracks?db=hg38&lastVirtModeType=default&lastVirtModeExtraState=&virtModeType=default&virtMode=0&nonVirtPosition=&position=chr6%3A166055376%2D166285375&hgsid=1668196600\\_TyrXKpANjNulE9hJyKBqwmyA2yA](https://genome.ucsc.edu/cgi-bin/hgTracks?db=hg38&lastVirtModeType=default&lastVirtModeExtraState=&virtModeType=default&virtMode=0&nonVirtPosition=&position=chr6%3A166055376%2D166285375&hgsid=1668196600_TyrXKpANjNulE9hJyKBqwmyA2yA)

757 The *hg19* UCSC browser session can be found here: [https://genome.ucsc.edu/cgi-bin/hgTracks?db=hg19&lastVirtModeType=default&lastVirtModeExtraState=&virtModeType=default&virtMode=0&nonVirtPosition=&position=chr6%3A166464129%2D166694128&hgsid=1668176188\\_UwkZBA1qkTeo3E3sO1Y0MYI3FJC3](https://genome.ucsc.edu/cgi-bin/hgTracks?db=hg19&lastVirtModeType=default&lastVirtModeExtraState=&virtModeType=default&virtMode=0&nonVirtPosition=&position=chr6%3A166464129%2D166694128&hgsid=1668176188_UwkZBA1qkTeo3E3sO1Y0MYI3FJC3)

758 The mouse (*mm10*) UCSC browser session can be found here: [https://genome.ucsc.edu/cgi-bin/hgTracks?db=mm10&lastVirtModeType=default&lastVirtModeExtraState=&virtModeType=default&virtMode=0&nonVirtPosition=&position=chr17%3A8368806%2D8468805&hgsid=1670749280\\_ioGL9AfZ5ZfCwVzWxcAwM4s0PHxk](https://genome.ucsc.edu/cgi-bin/hgTracks?db=mm10&lastVirtModeType=default&lastVirtModeExtraState=&virtModeType=default&virtMode=0&nonVirtPosition=&position=chr17%3A8368806%2D8468805&hgsid=1670749280_ioGL9AfZ5ZfCwVzWxcAwM4s0PHxk)

770 The Monodelphis (*monDom5*) UCSC browser session can be found here: [https://genome.ucsc.edu/cgi-bin/hgTracks?db=monDom5&lastVirtModeType=default&lastVirtModeExtraState=&virtModeType=default&virtMode=0&nonVirtPosition=&position=chr2%3A449921917%2D450073916&hgsid=1668178122\\_QQzeb4abeiOPvFBlo1AeXQ56AAQr](https://genome.ucsc.edu/cgi-bin/hgTracks?db=monDom5&lastVirtModeType=default&lastVirtModeExtraState=&virtModeType=default&virtMode=0&nonVirtPosition=&position=chr2%3A449921917%2D450073916&hgsid=1668178122_QQzeb4abeiOPvFBlo1AeXQ56AAQr)

771 The spotted gar (*GCF\_000242695.1*) UCSC browser session can be found here:  
[https://genome.ucsc.edu/cgi-bin/hgTracks?db=hub\\_2243239\\_GCF\\_000242695.1&lastVirtModeType=default&lastVirtModeExtraState=&virtModeType=default&virtMode=0&nonVirtPosition=&position=chrLG16%3A15070915%2D15148914&hgsid=1668181420\\_WCqDJoX4D50Wvt0W5P7oYAFrAjcN](https://genome.ucsc.edu/cgi-bin/hgTracks?db=hub_2243239_GCF_000242695.1&lastVirtModeType=default&lastVirtModeExtraState=&virtModeType=default&virtMode=0&nonVirtPosition=&position=chrLG16%3A15070915%2D15148914&hgsid=1668181420_WCqDJoX4D50Wvt0W5P7oYAFrAjcN)

772 The zebrafish (*danRer11*) UCSC browser session can be found here: [https://genome.ucsc.edu/cgi-bin/hgTracks?db=danRer11&lastVirtModeType=default&lastVirtModeExtraState=&virtModeType=default&virtMode=0&nonVirtPosition=&position=chr13%3A4394240%2D4472239&hgsid=1668178552\\_e2IT5zOIZFk3BhQoKpd0yek6naG5](https://genome.ucsc.edu/cgi-bin/hgTracks?db=danRer11&lastVirtModeType=default&lastVirtModeExtraState=&virtModeType=default&virtMode=0&nonVirtPosition=&position=chr13%3A4394240%2D4472239&hgsid=1668178552_e2IT5zOIZFk3BhQoKpd0yek6naG5)

773 Plasmids, stable transgenic zebrafish lines, and mouse knockout lines are available from the corresponding authors upon reasonable request.

784

785

786

787 **References**

788

- 789 1. Stemple, D. L. Structure and function of the notochord: an essential organ for chordate development. *Development* **132**, 2503–12 (2005).
- 790 2. Corallo, D., Trapani, V. & Bonaldo, P. The notochord: structure and functions. *Cell Mol Life Sci* **72**, 2989–3008 (2015).
- 791 3. Wang, F. *et al.* The embryonic and evolutionary boundaries between notochord and cartilage: A new look at nucleus pulposus-specific markers. *Osteoarthritis Cartilage* (2018) doi:10.1016/j.joca.2018.05.022.
- 792 4. Risbud, M. V., Schaer, T. P. & Shapiro, I. M. Toward an understanding of the role of notochordal cells in the adult intervertebral disc: from discord to accord. *Dev Dyn* **239**, 2141–8 (2010).
- 793 5. Bagnat, M. & Gray, R. S. Development of a straight vertebrate body axis. *Development (Cambridge, England)* vol. 147 Preprint at <https://doi.org/10.1242/dev.175794> (2020).
- 794 6. Stosiek, P., Kasper, M. & Karsten, U. Expression of cytokeratin and vimentin in nucleus pulposus cells. *Differentiation* **39**, 78–81 (1988).
- 795 7. Peck, S. H. *et al.* Whole Transcriptome Analysis of Notochord-Derived Cells during Embryonic Formation of the Nucleus Pulposus. *Scientific Reports* **2017** *7:17*, 1–14 (2017).
- 796 8. Satoh, N., Tagawa, K. & Takahashi, H. How was the notochord born? *14*, 56–75 (2012).
- 797 9. Dobrovolskaia-Zavadskia, N. Sur la mortification spontanee de la chez la souris nouveau-née et sur l'existence d'un caractere (facteur) hereditaire, non-viable. *Crit Rev Soc Biol* **97**, 114–116 (1927).
- 798 10. Corbo, J. C., Levine, M. & Zeller, R. W. Characterization of a notochord-specific enhancer from the Brachyury promoter region of the ascidian, *Ciona intestinalis*. *Development* **124**, 589–602 (1997).
- 799 11. Herrmann, B. G. The mouse Brachyury (T) gene. *Semin Dev Biol* **6**, 385–394 (1995).
- 800 12. Holland, P. W., Koschorz, B., Holland, L. Z. & Herrmann, B. G. Conservation of Brachyury (T) genes in amphioxus and vertebrates: developmental and evolutionary implications. *Development* **121**, 4283–4291 (1995).
- 801 13. Schulte-Merker, S., van Eeden, F. J., Halpern, M. E., Kimmel, C. B. & Nüsslein-Volhard, C. no tail (ntl) is the zebrafish homologue of the mouse T (Brachyury) gene. *Development* **120**, 1009–15 (1994).
- 802 14. Smith, J. C., Price, B. M. J. J., Green, J. B. A. A., Weigel, D. & Herrmann, B. G. Expression of a *xenopus* homolog of Brachyury (T) is an immediate-early response to mesoderm induction. *Cell* **67**, 79–87 (1991).
- 803 15. Halpern, M. E., Ho, R. K., Walker, C. & Kimmel, C. B. Induction of muscle pioneers and floor plate is distinguished by the zebrafish no tail mutation. *Cell* **75**, 99–111 (1993).
- 804 16. Rivera-Pérez, J. A. & Magnuson, T. Primitive streak formation in mice is preceded by localized activation of Brachyury and Wnt3. *Dev Biol* **288**, 363–371 (2005).
- 805 17. Martin, B. L. & Kimelman, D. Regulation of Canonical Wnt Signaling by Brachyury Is Essential for Posterior Mesoderm Formation. *Dev Cell* **15**, 121–133 (2008).
- 806 18. Henrique, D., Abrantes, E., Verrier, L. & Storey, K. G. Neuromesodermal progenitors and the making of the spinal cord. *Development* **142**, 2864–2875 (2015).
- 807 19. Schwaner, M. J., Hsieh, S. T., Swalla, B. J. & McGowan, C. P. An Introduction to an Evolutionary Tail: EvoDevo, Structure, and Function of Post-Anal Appendages. *Integr Comp Biol* **61**, 352–357 (2021).

830 20. Sebé-Pedrós, A. *et al.* Early evolution of the T-box transcription factor family. *Proc Natl Acad Sci U S*  
831 **A** **110**, 16050–16055 (2013).

832 21. Inoue, J., Yasuoka, Y., Takahashi, H. & Satoh, N. The chordate ancestor possessed a single copy of  
833 the Brachyury gene for notochord acquisition. *Zoological Lett* **3**, 1–7 (2017).

834 22. Amemiya, C. T. *et al.* The African coelacanth genome provides insights into tetrapod evolution.  
835 *Nature* **2013** **496**:7445 **496**, 311–316 (2013).

836 23. Harvey, S. A. A. *et al.* no tail integrates two modes of mesoderm induction. *Development* **137**, 1127–  
837 1135 (2010).

838 24. Clements, D., Taylor, H. C., Herrmann, B. G. & Stott, D. Distinct regulatory control of the Brachyury  
839 gene in axial and non-axial mesoderm suggests separation of mesoderm lineages early in mouse  
840 gastrulation. *Mech Dev* **56**, 139–149 (1996).

841 25. Latinkic, B. V. *et al.* The Xenopus Brachyury promoter is activated by FGF and low concentrations  
842 of activin and suppressed by high concentrations of activin and by paired-type homeodomain proteins.  
843 *Genes Dev* **11**, 3265–3276 (1997).

844 26. Arnold, S. J. *et al.* Brachyury is a target gene of the Wnt/β-catenin signaling pathway. *Mech Dev* **91**,  
845 249–258 (2000).

846 27. Schifferl, D. *et al.* A 37 kb region upstream of Brachyury comprising a notochord enhancer is  
847 essential for notochord and tail development. *Development* (2021) doi:10.1242/DEV.200059.

848 28. Farley, E. K., Olson, K. M., Zhang, W., Rokhsar, D. S. & Levine, M. S. Syntax compensates for poor  
849 binding sites to encode tissue specificity of developmental enhancers. *Proc Natl Acad Sci U S A* **113**,  
850 6508–13 (2016).

851 29. Song, B. P. *et al.* Diverse logics and grammar encode notochord enhancers. *Cell Rep* **42**, (2023).

852 30. Yakkou, Y., van Overbeeke, J. J., Santegoeds, R., van Engeland, M. & Temel, Y. The origin of  
853 chordoma. *Biochim Biophys Acta* (2014) doi:10.1016/j.bbcan.2014.07.012.

854 31. Nibu, Y., Jose-Edwards, D. S., Di Gregorio, A., Jos??-Edwards, D. S. & Di Gregorio, A. *From*  
855 *notochord formation to hereditary chordoma: The many roles of brachyury*. *BioMed Research*  
856 *International* vol. 2013 826435 (2013).

857 32. Vujovic, S. *et al.* Brachyury, a crucial regulator of notochordal development, is a novel biomarker for  
858 chordomas. *J Pathol* **209**, 157–165 (2006).

859 33. Bhadra, A. K. & Casey, A. T. Familial chordoma. A report of two cases. *J Bone Joint Surg Br* **88**,  
860 634–636 (2006).

861 34. Yang, X. R. *et al.* T (brachyury) gene duplication confers major susceptibility to familial chordoma.  
862 *Nat Genet* **41**, 1176–1178 (2009).

863 35. Hsu, W. *et al.* Generation of chordoma cell line JHC7 and the identification of Brachyury as a novel  
864 molecular target. *J Neurosurg* **115**, 760–769 (2011).

865 36. Nelson, A. C. *et al.* An integrated functional genomics approach identifies the regulatory network  
866 directed by brachyury (T) in chordoma. *Journal of Pathology* **228**, 274–285 (2012).

867 37. Tarpey, P. S. *et al.* The driver landscape of sporadic chordoma. *Nat Commun* **8**, 1–6 (2017).

868 38. Hsu, W. *et al.* Generation of chordoma cell line JHC7 and the identification of Brachyury as a novel  
869 molecular target. *J Neurosurg* **115**, 760–769 (2011).

870 39. Tarpey, P. S. *et al.* The driver landscape of sporadic chordoma. *Nat Commun* **8**, 1–6 (2017).

871 40. Sharifnia, T. *et al.* Small-molecule targeting of brachyury transcription factor addiction in chordoma.  
872 *Nat Med* **1** (2019) doi:10.1038/s41591-018-0312-3.

873 41. Nelson, A. C. *et al.* An integrated functional genomics approach identifies the regulatory network  
874 directed by brachyury (T) in chordoma. *Journal of Pathology* **228**, 274–285 (2012).

875 42. Beisaw, A. *et al.* BRACHYURY directs histone acetylation to target loci during mesoderm  
876 development. *EMBO Rep* **19**, 118 (2018).

877 43. Faial, T. *et al.* Brachyury and SMAD signalling collaboratively orchestrate distinct mesoderm and  
878 endoderm gene regulatory networks in differentiating human embryonic stem cells. *Development*  
879 **142**, 2121 (2015).

880 44. Mikkelsen, T. S. *et al.* Genome of the marsupial *Monodelphis domestica* reveals innovation in non-  
881 coding sequences. *Nature* **447**, 167–77 (2007).

882 45. Kemmler, C. L. *et al.* Next-generation plasmids for transgenesis in zebrafish and beyond.  
883 *Development* **150**, (2023).

884 46. Nowoshilow, S. *et al.* The axolotl genome and the evolution of key tissue formation regulators.  
885 *Nature* **2018** **554**:7690 **554**, 50–55 (2018).

886 47. Prummel, K. D. *et al.* A conserved regulatory program initiates lateral plate mesoderm emergence  
887 across chordates. *Nat Commun* **10**, 3857 (2019).

888 48. Kwon, E. Z. *et al.* Comprehensive In Vivo Interrogation Reveals Phenotypic Impact of Human  
889 Enhancer Variants. *Cell* **180**, 1262 (2020).

890 49. Grant, C. E., Bailey, T. L. & Noble, W. S. FIMO: scanning for occurrences of a given motif.  
891 *Bioinformatics* **27**, 1017 (2011).

892 50. Pippucci, T. *et al.* Mutations in the 5' UTR of ANKRD26, the ankirin repeat domain 26 gene, cause  
893 an autosomal-dominant form of inherited thrombocytopenia, THC2. *Am J Hum Genet* **88** 1, 115–120  
894 (2011).

895 51. Nei, M., Xu, P. & Glazko, G. Estimation of divergence times from multiprotein sequences for a few  
896 mammalian species and several distantly related organisms. *Proceedings of the National Academy  
897 of Sciences* **98**, 2497–2502 (2001).

898 52. Goodstadt, L., Heger, A., Webber, C. & Ponting, C. P. An analysis of the gene complement of a  
899 marsupial, *Monodelphis domestica*: evolution of lineage-specific genes and giant chromosomes.  
900 *Genome Res* **17**, 969–981 (2007).

901 53. Kumar, S., Stecher, G., Suleski, M. & Blair Hedges, S. TimeTree: A Resource for Timelines,  
902 Timetrees, and Divergence Times. *Mol Biol Evol* **34**, 1812–1819 (2017).

903 54. Passamaneck, Y. J. *et al.* Direct activation of a notochord cis-regulatory module by Brachyury and  
904 FoxA in the ascidian *Ciona intestinalis*. *Development* **136**, 3679–3689 (2009).

905 55. Gluecksohn-Schoenheimer, S. THE DEVELOPMENT OF TWO TAILLESS MUTANTS IN THE  
906 HOUSE MOUSE. *Genetics* **23**, 573–584 (1938).

907 56. Gluecksohn-Schoenheimer, S. The Development of Normal and Homozygous Brachy (T/T) Mouse  
908 Embryos in the Extraembryonic Coelom of the Chick. *Proceedings of the National Academy of  
909 Sciences* **30**, 134–140 (1944).

910 57. Yanagisawa, K. O. Does the T gene determine the anteroposterior axis of a mouse embryo? *The  
911 Japanese Journal of Genetics* **65**, 287–297 (1990).

912 58. Pennimpede, T. *et al.* In vivo knockdown of Brachyury results in skeletal defects and urorectal  
913 malformations resembling caudal regression syndrome. *Dev Biol* **372**, 55–67 (2012).

914 59. Zhu, J., Kwan, K. M. & Mackem, S. Putative oncogene Brachyury (T) is essential to specify cell fate  
915 but dispensable for notochord progenitor proliferation and EMT. *Proc Natl Acad Sci U S A*  
916 1601252113- (2016) doi:10.1073/pnas.1601252113.

917 60. Dobrovolskaia-Zavadskia, N. Sur la mortification spontanee de la chez la souris nouveau-née et sur  
918 l'existence d'un caractere (facteur) hereditaire, non-viable. *Crit Rev Soc Biol* **97**, 114–116 (1927).

919 61. Nibu, Y., Jose-Edwards, D. S., Di Gregorio, A., Jos??-Edwards, D. S. & Di Gregorio, A. *From  
920 notochord formation to hereditary chordoma: The many roles of brachyury*. *BioMed Research  
921 International* vol. 2013 826435 (2013).

922 62. Martin, B. L. & Kimelman, D. Brachyury establishes the embryonic mesodermal progenitor niche.  
923 *Genes Dev* **24**, 2778–83 (2010).

924 63. Braasch, I. *et al.* The spotted gar genome illuminates vertebrate evolution and facilitates human-  
925 teleost comparisons. *Nat Genet* **48**, 427–437 (2016).

926 64. Thompson, A. W. *et al.* The bowfin genome illuminates the developmental evolution of ray-finned  
927 fishes. *Nature Genetics* 2021 1–12 (2021) doi:10.1038/s41588-021-00914-y.

928 65. Bradley Shaffer, H. *et al.* The western painted turtle genome, a model for the evolution of extreme  
929 physiological adaptations in a slowly evolving lineage. *Genome Biol* **14**, (2013).

930 66. Takezaki, N. Global Rate Variation in Bony Vertebrates. *Genome Biol Evol* **10**, 1803–1815 (2018).

931 67. Kvon, E. Z. *et al.* Enhancer redundancy in development and disease. **22**, (2021).

932 68. Letelier, J. *et al.* A conserved Shh cis-regulatory module highlights a common developmental origin  
933 of unpaired and paired fins. *Nat Genet* **50**, 504–509 (2018).

934 69. Cannavò, E. *et al.* Shadow Enhancers Are Pervasive Features of Developmental Regulatory  
935 Networks. *Curr Biol* (2015) doi:10.1016/j.cub.2015.11.034.

936 70. Hong, J. W., Hendrix, D. A. & Levine, M. S. Shadow enhancers as a source of evolutionary novelty.  
937 *Science* (1979) **321**, 1314 (2008).

938 71. Antosova, B. *et al.* The Gene Regulatory Network of Lens Induction Is Wired through Meis-  
939 Dependent Shadow Enhancers of Pax6. *PLoS Genet* **12**, e1006441 (2016).

940 72. Osterwalder, M. *et al.* Enhancer redundancy provides phenotypic robustness in mammalian  
941 development. *Nature* **554**, 239–243 (2018).

942 73. Hong, J. W., Hendrix, D. A. & Levine, M. S. Shadow enhancers as a source of evolutionary novelty.  
943 *Science* (1979) **321**, 1314 (2008).

944 74. Irimia, M. *et al.* Extensive conservation of ancient microsynteny across metazoans due to cis-  
945 regulatory constraints. *Genome Res* **22**, 2356–2367 (2012).

946 75. Amacher, S. L., Draper, B. W., Summers, B. R. & Kimmel, C. B. The zebrafish T-box genes no tail  
947 and spadetail are required for development of trunk and tail mesoderm and medial floor plate.  
948 *Development* 3311–3323 (2002) doi:10.1242/DEV.129.14.3311.

949 76. Rennebeck, G. M. *et al.* Is there a Brachyury the Second? Analysis of a transgenic mutation involved  
950 in notochord maintenance in mice. *Dev Biol* **172**, 206–217 (1995).

951 77. Rennebeck, G., Lader, E., Fujimoto, A., Lei, E. P. & Artzt, K. Mouse Brachyury the second (T2) is a  
952 gene next to classical T and a candidate gene for tct. *Genetics* **150**, 1125–1131 (1998).

953 78. Takei, H. & Powell, S. Z. Novel immunohistochemical markers in the diagnosis of nonglial tumors of  
954 nervous system. *Adv Anat Pathol* **17**, 150–153 (2010).

955 79. Sangi, A. R. *et al.* Specificity of brachyury in the distinction of chordoma from clear cell renal cell  
956 carcinoma and germ cell tumors: a study of 305 cases. *Mod Pathol* **24**, 425–429 (2011).

957 80. Heaton, J. M. & Turner, D. R. Reflections on notochordal differentiation arising from a study of  
958 chordomas. *Histopathology* **9**, 543–550 (1985).

959 81. Choi, K. S., Cohn, M. J. & Harfe, B. D. Identification of nucleus pulposus precursor cells and  
960 notochordal remnants in the mouse: implications for disk degeneration and chordoma formation. *Dev  
961 Dyn* **237**, 3953–3958 (2008).

962 82. Tang, X., Jing, L. & Chen, J. Changes in the Molecular Phenotype of Nucleus Pulposus Cells with  
963 Intervertebral Disc Aging. *PLoS One* **7**, 52020 (2012).

964 83. Richardson, S. M. *et al.* Notochordal and nucleus pulposus marker expression is maintained by sub-  
965 populations of adult human nucleus pulposus cells through aging and degeneration. *Scientific  
966 Reports* **2017** *7:1* 7, 1–11 (2017).

967 84. Nakamichi, R. & Asahara, H. The transcription factors regulating intervertebral disc development.  
968 *JOR Spine* **3**, e1081 (2020).

969 85. Hu, Y., Mintz, A., Shah, S. R. R., Quinones-Hinojosa, A. & Hsu, W. The FGFR/MEK/ERK/brachyury  
970 pathway is critical for chordoma cell growth and survival. *Carcinogenesis* **35**, 1491–1499 (2014).

971 86. D'Agati, G. *et al.* Active receptor tyrosine kinases, but not Brachyury, are sufficient to trigger  
972 chordoma in zebrafish. *Dis Model Mech* **12**, (2019).

973 87. Presneau, N. *et al.* Role of the transcription factor T (brachyury) in the pathogenesis of sporadic  
974 chordoma: a genetic and functional-based study. *J Pathol* **223**, 327–335 (2011).

975 88. Brink, S. C. van den *et al.* Single-cell and spatial transcriptomics reveal somitogenesis in gastruloids.  
976 *Nature* **2020** 1–5 (2020) doi:10.1038/s41586-020-2024-3.

977 89. López López-Anguita, N. *et al.* Hypoxia induces an early primitive streak signature, enhancing  
978 spontaneous elongation and lineage representation in gastruloids. *Development* **149**, (2022).

979 90. Veenvliet, J. V. *et al.* Mouse embryonic stem cells self-organize into trunk-like structures with neural  
980 tube and somites. *Science* (1979) **370**, (2020).

981 91. Moris, N. *et al.* An in vitro model of early anteroposterior organization during human development.  
982 *Nature* 1–6 (2020) doi:10.1038/s41586-020-2383-9.

983 92. Xu, P. F. *et al.* Construction of a mammalian embryo model from stem cells organized by a  
984 morphogen signalling centre. *Nat Commun* **12**, (2021).

985 93. Xu, P.-F., Houssin, N., Ferri-Lagneau, K. F., Thisse, B. & Thisse, C. Construction of a vertebrate  
986 embryo from two opposing morphogen gradients. *Science* **344**, 87–9 (2014).

987 94. Rito, T., Libby, A. R. G., Demuth, M. & Briscoe, J. Notochord and axial progenitor generation by  
988 timely BMP and NODAL inhibition during vertebrate trunk formation. *bioRxiv* 2023.02.27.530267  
989 (2023) doi:10.1101/2023.02.27.530267.

990 95. Tosic, J. *et al.* Eomes and Brachyury control pluripotency exit and germ-layer segregation by  
991 changing the chromatin state. *Nat Cell Biol* **21**, 1518–1531 (2019).

992 96. Koch, F. *et al.* Antagonistic Activities of Sox2 and Brachyury Control the Fate Choice of Neuro-  
993 Mesodermal Progenitors. *Dev Cell* (2017) doi:10.1016/j.devcel.2017.07.021.

994 97. Abascal, F. *et al.* Expanded encyclopaedias of DNA elements in the human and mouse genomes.  
995 *Nature* **583**, 699–710 (2020).

996 98. Mosimann, C. Multisite Gateway Calculations: Excel spreadsheet. *protocols.io* Preprint at  
997 <https://doi.org/10.17504/protocols.io.b4xdqxi6> (2022).

998 99. Westerfield, M. *The Zebrafish Book: a guide for the laboratory use of zebrafish (Danio rerio)*.  
999 (University of Oregon Press, 2007).

000 100. Mosimann, C. *et al.* Ubiquitous transgene expression and Cre-based recombination driven by the  
001 ubiquitin promoter in zebrafish. *Development* **138**, 169–177 (2011).

002 101. Kwan, K. M. *et al.* The Tol2kit: a multisite gateway-based construction kit for Tol2 transposon  
003 transgenesis constructs. *Dev Dyn* **236**, 3088–3099 (2007).

004 102. Felker, A. & Mosimann, C. Contemporary zebrafish transgenesis with Tol2 and application for  
005 Cre/lox recombination experiments. *Methods Cell Biol* **135**, 219–44 (2016).

006 103. Yun, M. H., Gates, P. B. & Brookes, J. P. Regulation of p53 is critical for vertebrate limb  
007 regeneration. *Proc Natl Acad Sci U S A* **110**, 17392–17397 (2013).

008 104. Khattak, S. *et al.* Optimized axolotl (*Ambystoma mexicanum*) husbandry, breeding, metamorphosis,  
009 transgenesis and tamoxifen-mediated recombination. *Nat Protoc* **9**, 529–540 (2014).

010 105. Armstrong, J. B. & Malacinski, G. M. Developmental biology of the axolotl. 320 (1989).

011 106. Hippenmeyer, S. *et al.* Genetic Mosaic Dissection of Lis1 and Ndel1 in Neuronal Migration. *Neuron*  
012 **68**, 695 (2010).

013 107. Tasic, B. *et al.* Site-specific integrase-mediated transgenesis in mice via pronuclear injection. *Proc  
014 Natl Acad Sci U S A* **108**, 7902–7 (2011).

015 108. Osterwalder, M. *et al.* Characterization of Mammalian In Vivo Enhancers Using Mouse Transgenesis  
016 and CRISPR Genome Editing. *Methods in Molecular Biology* **2403**, 147–186 (2022).

017 109. Farley, E. K. *et al.* Suboptimization of developmental enhancers. *Science* **350**, 325–8 (2015).

018 110. Harafuji, N., Keys, D. N. & Levine, M. Genome-wide identification of tissue-specific enhancers in the  
019 Ciona tadpole. *Proc Natl Acad Sci U S A* **99**, 6802–6805 (2002).

020 111. Christiaen, L., Wagner, E., Shi, W. & Levine, M. Electroporation of Transgenic DNAs in the Sea  
021 Squirt Ciona. *Cold Spring Harb Protoc* **2009**, pdb.prot5345 (2009).

022 112. Jenickova, I. *et al.* Efficient allele conversion in mouse zygotes and primary cells based on  
023 electroporation of Cre protein. *Methods* **191**, 87–94 (2021).

024 113. Mašek, J., Machoň, O., Kořínek, V., Taketo, M. M. & Kozmík, Z. Tcf7l1 protects the anterior neural  
025 fold from adopting the neural crest fate. *Development* **143**, 2206–2216 (2016).

026 114. Bradley Shaffer, H. *et al.* The western painted turtle genome, a model for the evolution of extreme  
027 physiological adaptations in a slowly evolving lineage. *Genome Biol* **14**, (2013).

028 115. Martin, F. J. *et al.* Ensembl 2023. *Nucleic Acids Res* **51**, D933–D941 (2023).

029 116. Katoh, K., Asimenos, G. & Toh, H. Multiple alignment of DNA sequences with MAFFT. *Methods Mol  
030 Biol* **537**, 39–64 (2009).

031 117. Grant, C. E., Bailey, T. L. & Noble, W. S. FIMO: scanning for occurrences of a given motif.  
032 *Bioinformatics* **27**, 1017 (2011).

033 118. Castro-Mondragon, J. A. *et al.* JASPAR 2022: the 9th release of the open-access database of  
034 transcription factor binding profiles. *Nucleic Acids Res* **50**, D165–D173 (2022).

035 119. Christiaen, L., Wagner, E., Shi, W. & Levine, M. Electroporation of Transgenic DNAs in the Sea  
036 Squirt Ciona. *Cold Spring Harb Protoc* **2009**, pdb.prot5345 (2009).

037 120. Mašek, J., Machoň, O., Kořínek, V., Taketo, M. M. & Kozmík, Z. Tcf7l1 protects the anterior neural  
038 fold from adopting the neural crest fate. *Development* **143**, 2206–2216 (2016).

039 121. Kemmler, C. L. *et al.* Next-generation plasmids for transgenesis in zebrafish and beyond.  
040 *Development* **150**, (2023).

041 122. Prummel, K. D. *et al.* A conserved regulatory program initiates lateral plate mesoderm emergence  
042 across chordates. *Nat Commun* **10**, 3857 (2019).

043 123. Visel, A., Minovitsky, S., Dubchak, I. & Pennacchio, L. A. VISTA Enhancer Browser--a database of  
044 tissue-specific human enhancers. *Nucleic Acids Res* **35**, (2007).

045

046

047 **Acknowledgements**

048 We thank Christine Archer, Molly Waters, Nikki Tsuji, Ainsley Gilbard, and Olivia Gomez (CU Anschutz), as  
049 well as Vesna Barros, Lukas Obernosterer, and Yorgos Panayotou (UZH) for excellent zebrafish husbandry  
050 support; Jitka Lachova (IMG) for outstanding expert assistance with mouse embryo preparation and strain  
051 maintenance; Beate Gruhl and Anja Wagner (TU Dresden) for excellent axolotl husbandry support; Dr. Alexa  
052 Sadier and Dr. Karen Sears (UCLA) for generously providing us with *Monodelphis* genomic DNA; Dr. Jelena  
053 Kresoja and Elena Cabello for bioinformatics input; and all members of our individual laboratories for critical  
054 input and discussion on experiments, concepts, and the manuscript. The species silhouettes were adapted  
055 from the PhyloPic database ([www.phylopic.org](http://www.phylopic.org)). This work has been supported by an UZH URPP  
056 “Translational Cancer Research” seed grant and NIH/NIDDK grant 1R01DK129350-01A1 to A.B.; the  
057 Children’s Hospital Colorado Foundation, National Science Foundation Grant 2203311, and Swiss National  
058 Science Foundation (SNSF) Sinergia grant CRSII5\_180345 to C.M.; a project grant from the Swiss Cancer  
059 League, the SwissBridge Award 2016 from the SwissBridge Foundation, Additional Ventures SVRF2021-  
060 1048003 grant, and the University of Colorado Anschutz Medical Campus to C.M. and A.B.; NIH/NIGMS  
061 1T32GM141742-01, 3T32GM121742-02S1, and NIH/NHLBI F31HL167580 to H.R.M.; Czech Science  
062 Foundation grant 23-07056S to Z.K. and Czech Center for Phenogenomics infrastructure support  
063 LM2018126, OP VaVpI CZ.1.05/2.1.00/19.0395, and CZ.1.05/1.1.00 /02.0109 to IMG; NIH grant  
064 5R01DE024745-09 to L.S.; NSF EDGE Award #2029216 to I.B.; SNSF Eccellenza professorship  
065 PCEFP3\_186993 to M.O.; an Alexander von Humboldt postdoctoral Fellowship to A.C.; Deutsche  
066 Forschungsgemeinschaft (DFG) Grants 22137416, 450807335 and 497658823, as well as TUD and CRTD  
067 funds to M.H.Y.; NIH grant DP2HG010013 to E.K.F and F.L.; NIH grants R01HG003988, R01DE028599,

068 and R01HL162304 to A.V. and B.J.M.  
069  
070

071 **Author Contributions**

072 C.L.K., H.R.M., S.B., C.M. and A.B. – Zebrafish experiment design and performance, UCSC browser data  
073 analysis, manuscript writing. D.K., A.C. and M.H.Y. – Axolotl experiment design and performance, data  
074 analysis, manuscript writing. B.M., V.R., A.V. and M.O. – Mouse enhancer testing experiment design and  
075 performance, data analysis, manuscript writing. V.H.A. and L.S. – Design and performance of experiments  
076 to assess enhancer activity on mouse embryonic sections, histology, data analysis, manuscript writing. F.L.  
077 and E.F. – Ciona experiment design and performance, data analysis, manuscript writing. J.S. and Z.K. –  
078 Mouse CRISPR-Cas9 knockout experiment design and performance, data analysis, manuscript writing.  
079 O.E.F. and I.B. – Bridge species research design, data analysis, manuscript writing.  
080  
081

082 **Competing Interests**

083 The authors declare no competing interests.  
084  
085  
086

087 **Figure 1: Human *Brachyury* enhancer elements *T3*, *C* and *I* are active in different species.**

088 (A) Human *Brachyury*/T/TBXTB locus with surrounding gene loci adapted from UCSC genome browser.  
089 Repeats marked in black using the RepeatMasker track; additional tracks include the ENCODE conserved  
090 *cis*-regulatory elements (cCREs) and layered H3K27ac signals. Further annotated are approximate  
091 amplifications (light orange) and the minimally amplified region (dark orange) in chordoma tumors. ATAC-  
092 sequencing (light blue peaks) and T ChIP-sequencing (dark blue lines) suggest enhancer elements (light  
093 pink highlight, not active; light blue highlight, active) that are conserved in mouse and the marsupial  
094 *Monodelphis domestica*.

095 (B,C,D) Representative F0 zebrafish embryos injected with the human enhancer elements *hs\_T3* (B), *hs\_C*  
096 (C), and *hs\_I* (D) showing mosaic *mCerulean* reporter expression in the notochord at 24 hpf and expression  
097 of *ubi:mCherry* as injection control. N represents the number of animals expressing *mCerulean* in the  
098 notochord relative to the total number of animals expressing *mCherry*. Scale bar in B: 0.5 mm, applies to B-C.  
099

100 (E,F,G) Representative images of stable transgenic F2 embryos at 48 hpf for each of the human enhancer  
101 elements *hs\_T3*, *hs\_C*, and *hs\_I* crossed to *Tg(drl:mCherry)* that labels lateral plate mesoderm and later  
102 cardiovascular lineages. Transgenic F2 embryos recapitulate the F0 expression pattern in the notochord,  
103 with *hs\_T3* (E) additionally expressing cerulean in the pharyngeal arches and fin, and *hs\_I* (G) in the proximal  
104 kidney close to the anal pore. Enhancer element *hs\_C* (F) stable transgenic lines have lower relative  
105 notochord reporter activity than *hs\_T3* and *hs\_I*. Scale bar in E: 0.5 mm, applies to E-G.  
106

107 (H,I,J) Representative F0 axolotl embryos at peri-hatching stages expressing *mCerulean* from the human  
108 enhancers *hs\_T3* (G), *hs\_C* (H), *hs\_I* (I). N represent the number of animals expressing *mCerulean* in the  
109 notochord relative to the total number of animals showing any *mCerulean* expression. Scale bar in H: 1 mm,  
110 applies to H-J.

111 (K,M,O) Representative images of transgenic E9.5 mouse embryos expressing *lacZ* (encoding beta-  
112 galactosidase) under the human enhancers *hs\_T3* (K), *hs\_C* (M), and *hs\_I* (O) visualized with X-gal whole-  
113 mount staining. While *hs\_C* and *hs\_I* express beta-galactosidase in the entire notochord, beta-galactosidase  
114 expression from *hs\_T3* is restricted to the posterior notochord. Black asterisk marks absence of beta-  
115 galactosidase in the anterior notochord. N represent the number of animals expressing beta-galactosidase  
116 in the notochord relative to the total number of animals with tandem integrations at H11. Dotted lines  
117 represent the sectioning plane. Scale bar in K: 0.5 mm, applies to K,M,O.

118 (L,N,P) Representative images of Fast Red-stained cross sections from embryos shown on the left, *hs\_T3*  
119 (L), *hs\_C* (N), and *hs\_I* (P). Black arrowheads point at notochord, and inserts show notochords at 2x higher  
120 magnification. Scale bar in L: 0.25 mm, applies to L,N,P. The species silhouettes were adapted from the  
121 PhyloPic database ([www.phylopic.org](http://www.phylopic.org)).  
122

123 **Figure 2: Identified TBXT binding sites in the enhancer elements are essential for reporter activity.**

124 (A) Sequence of the human TBXT binding site (T-box) using JASPAR.

125 (B) FIMO output with location of the T-box, statistical significance, and matched sequence within the  
126 enhancer elements. P values were calculated by FIMO which computes a log-likelihood ratio score for each  
127 position in the sequence, then converts this score to a P value, and then applies false discovery rate analysis

128 to estimate a Q value for each position.

129 (C) Schematic depiction of the wildtype human enhancer elements with the TBXT binding site/T-box (pink,  
130 red, purple boxes) and the enhancer elements without the respective T-box sites ( $\Delta Tbox$ ). The human  
131 enhancer elements are depicted in the reverse complement direction. Tbox130-145, Tbox277-292, Tbox309-  
132 324: p < 0.00008, Tbox184-199: p < 0.005, Tbox201-216: p < 0.008.

133 (D-I) Injection of the wildtype enhancer elements *hs\_T3* (D), *hs\_Cshort* (F), and *hs\_I* (H) as reporter  
134 constructs results in mApple fluorophore expression in the notochord at 48 hpf, whereas injection of  
135 *hs\_T3* $\Delta$ *Tbox* (E), *hs\_Cshort* $\Delta$ *Tbox* (G), and *hs\_I* $\Delta$ *Tbox* (I) show complete loss of notochord expression  
136 (asterisks in E,G,I). Arrowheads (D-I) mark EGFP expression in the pineal gland from the transgenesis  
137 marker *exorh:EGFP*. Scale bar in D: 0.5 mm, applies to D-I.

138

139

140 **Figure 3: Mouse *Brachyury* enhancer elements are active in different species.**

141 (A) Mouse *Brachyury/T/TBXTB* locus adapted from the UCSC genome browser. Repeats marked in black  
142 using the RepeatMasker track; additional tracks include the ENCODE cCREs, H3K27ac (yellow), H3K4me  
143 (red) and DNase (green) signals. ATAC-sequencing (light blue peaks) and T ChIP-sequencing (dark blue  
144 lines) indicate enhancer elements (light pink highlight, not active; light blue highlight, active) that are  
145 conserved in human and *Monodelphis*.

146 (B,C,D) Representative F0 zebrafish embryos injected with the mouse enhancer elements *mm\_T3* (B),  
147 *mm\_C* (C), and *mm\_I* (D). *mm\_T3* and *mm\_I* show mosaic *mCerulean* reporter expression in the notochord  
148 at 24 hpf and mosaic *ubi:mCherry* expression as injection control. Mouse enhancer element *mm\_C* is not  
149 active in the zebrafish notochord (asterisk in C). N represent the number of animals expressing mCerulean  
150 in the notochord relative to the total number of animals expressing mCherry. Scale bar in B: 0.5 mm, applies  
151 to B-D.

152 (E,G,I) Representative images of transgenic E9.5 mouse embryos expressing *lacZ* (encoding beta-  
153 galactosidase) under the mouse enhancer elements *mm\_T3* (E), *mm\_C* (G) and *mm\_I* (I) visualized with X-  
154 gal whole mount staining. While *mm\_T3* and *mm\_I* express beta-galactosidase in the entire notochord, beta-  
155 galactosidase expression from mouse *mm\_C* is absent (asterisk in G). N represent the number of animals  
156 expressing beta-galactosidase in the notochord relative to the total number of animals with tandem  
157 integrations at H11. Dotted lines represent the sectioning plane. Scale bar in E: 0.5 mm, applies to E,G,I.

158 (F,H,J) Representative images of Fast Red-stained cross sections from embryos shown on the left, *mm\_T3*  
159 (F), *mm\_C* (H), and *mm\_I* (J). Black arrowheads point at notochord, and inserts show notochords at 2x higher  
160 magnification. Scale bar in F: 0.25 mm, applies to F,H,J. The species silhouettes were adapted from the  
161 PhyloPic database ([www.phylopic.org](http://www.phylopic.org)).

162

163

164 **Figure 4: *Monodelphis Brachyury* enhancer elements are active in different species.**

165 (A) *Monodelphis Brachyury/T/TBXTB* locus adapted from the UCSC genome browser. Repeats are marked  
166 in black using the RepeatMasker track. Further annotated are tracks containing N-SCAN gene predictions  
167 and 9 Species Conservation. The light blue highlighted boxes mark the *Monodelphis* enhancer elements *T3*,  
168 *C* and *I* and their conservation in other species.

169 (B,C,D) Representative F0 zebrafish embryos injected with the *Monodelphis* enhancer elements *md\_T3* (B),  
170 *md\_C* (C), and *md\_I* (D) showing mosaic *mCerulean* reporter expression in the zebrafish notochord at 24  
171 hpf. *ubi:mCherry* was used as injection control. N represent the number of animals expressing mCerulean  
172 in the notochord relative to the total number of animals expressing mCherry. Scale bar in B: 0.5 mm, applies to  
173 B-C.

174 (E,F) Representative images of *Ciona* embryos electroporated with *Monodelphis* enhancer element *md\_C*  
175 (E), and minimal *forkhead* promoter (*fkh*) only as control (F). *Monodelphis* enhancer element *md\_C*  
176 expresses EGFP throughout the entire *Ciona* notochord, compared to minimal *fkh* promoter only which does  
177 not express EGFP at all (asterisk in F). N represent the number of animals expressing EGFP in the notochord  
178 relative to the total number of animals. Inserts on the top right represent bright field images of respective  
179 embryos. Scale bar in E: 0.05 mm, applies to E,F. The species silhouettes were adapted from the PhyloPic  
180 database ([www.phylopic.org](http://www.phylopic.org)).

181

182

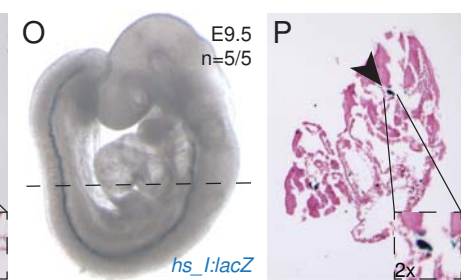
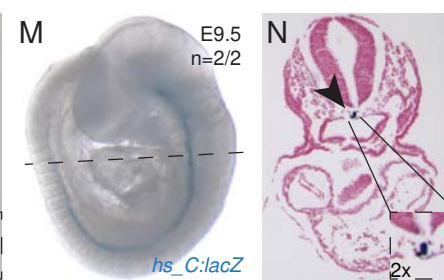
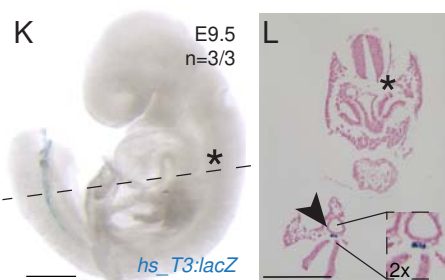
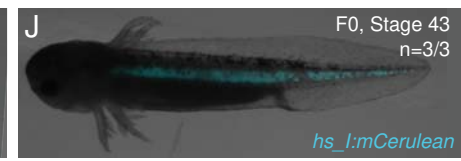
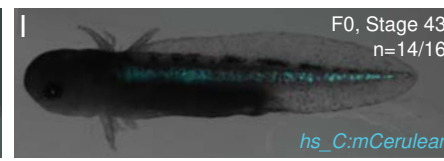
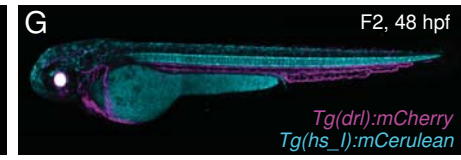
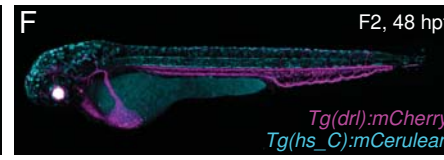
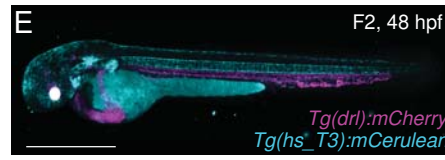
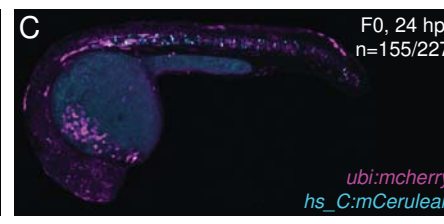
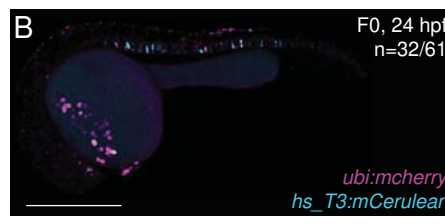
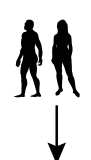
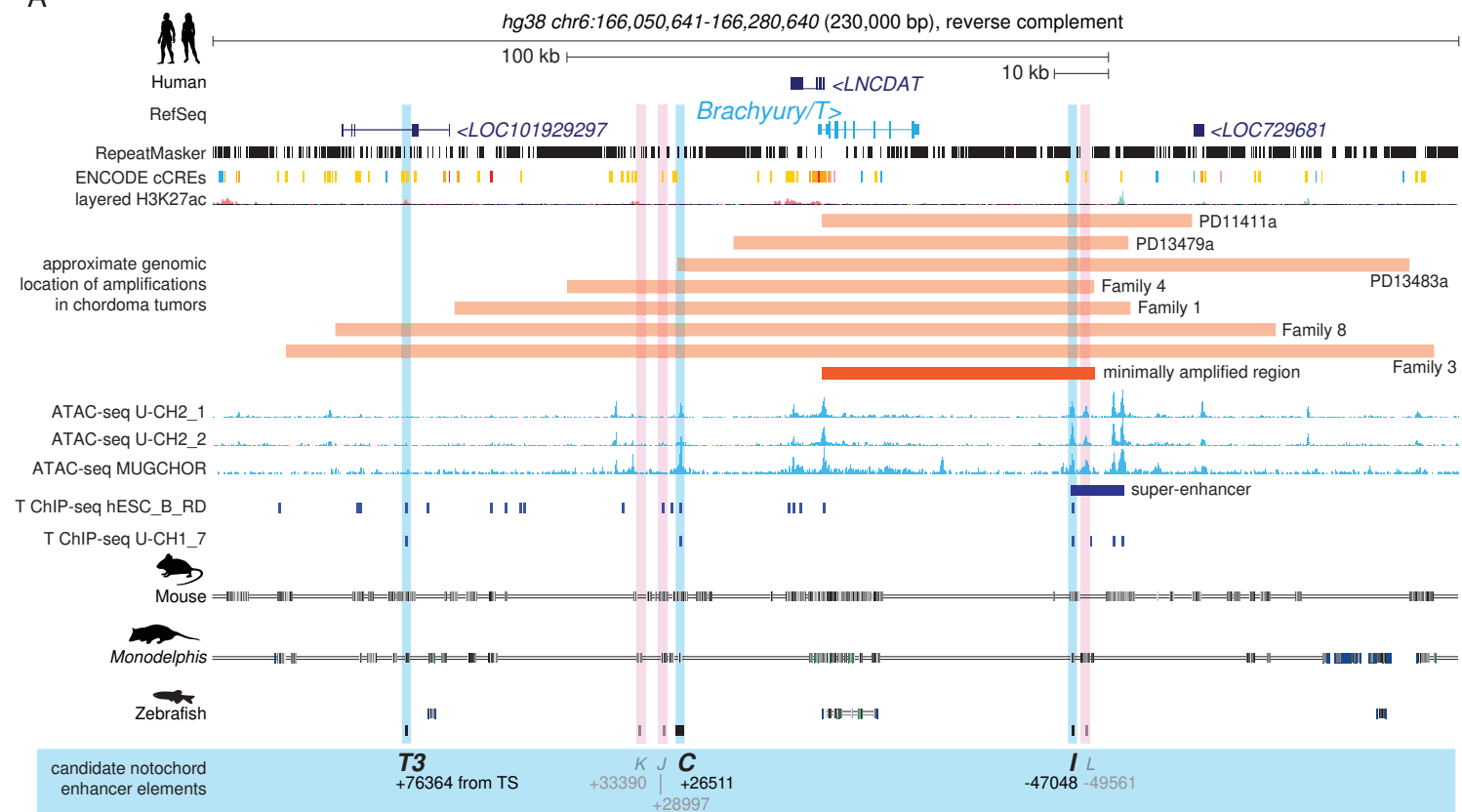
183 **Figure 5: Deletion of the three enhancer elements *T3*, *C* and *I* results in selective loss of *Brachyury*  
184 protein expression in the notochord at E9.5 and posterior defects at E12.5.**

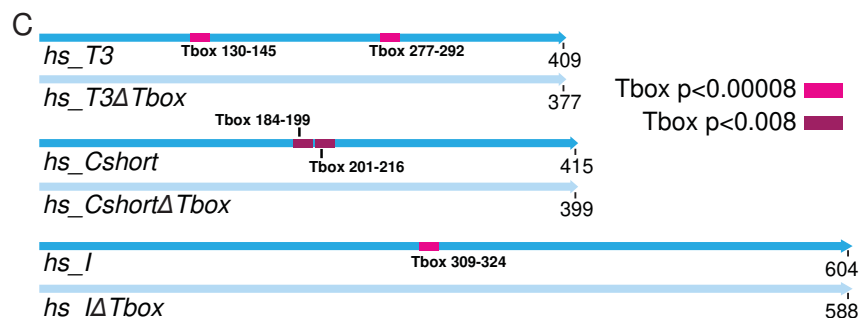
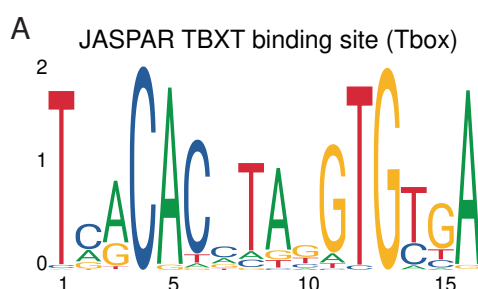
185 (A) Overview of wildtype mouse *Brachyury/T/TBXTB* locus adapted from the UCSC genome browser and  
186 deletion alleles generated with CRISPR-Cas9 genome editing. Exact coordinates and sequences of target  
187 sites, deletions, and genotyping primer sequences can be found in **Supplementary Data 5**.

188 (B-G) Brachyury/T antibody staining (red) of E9.5 embryos. White dashed square in panels represents  
189 location of right bottom inserts with 2x magnification. Brachyury/T protein expression in the notochord is  
190 dose-dependent on the three enhancer elements. Asterisks in D-G mark absent notochord in rostral portion  
191 of the embryo. Scale bar in B: 1 mm, applies to panels B-G.  
192 (H-M) Overall morphology of E12.5 embryos with different genotypes. Blue lines indicate the location of  
193 immunofluorescence and H&E sections. Spina bifida and tail defects are dose-dependent. Arrowheads mark  
194 rudimentary tails. White lines mark spina bifida. Scale bar in H: 1 mm, applies to panels H-M.  
195 (N-S) Dorsal view of embryos (sectioned at blue line in H-M). White lines mark areas of spina bifida.  
196 Arrowheads mark rudimentary tails compared to tails in wildtype control and double knock-out allele. Scale  
197 bar in N: 2.5 mm, applies to panels N-S.  
198 (T-Y) Immunofluorescence of mouse transverse sections. Anti-Sox2 labels the neural plate, anti-Tbx5 the  
199 notochord, and DAPI marks nuclei. Sox2 expression is comparable amongst all genotypes, even in the  
200 genotypes with spina bifida, while there is loss of Brachyury/T staining in the notochord with increased loss  
201 of the enhancers. Arrowheads point to notochord. Asterisks mark absent notochord. Scale bar in T: 0.2 mm,  
202 applies to panels T-Y.  
203 (Z-E') H&E staining of transverse sections confirm the dose-dependent loss of the notochord and spina bifida.  
204 Arrowheads point to notochord. Asterisks mark absent notochord. Scale bar in Z: 0.2 mm, applies to panels  
205 Z-E'.  
206  
207

208 **Figure 6: Bridge species establish the presence of *Tbx5b* enhancers across jawed vertebrates.**  
209 (A) Location of the enhancer elements in the human (top), gar (middle), and zebrafish (bottom)  
210 *Brachyury/T/Tbx5b* loci, adapted from the UCSC browser as established through the “gar bridge”.  
211 (B,C,D) Representative F0 zebrafish embryos injected with the gar enhancer elements *lo\_T3* (B), *lo\_C* (C),  
212 and *lo\_I* (D). *T3* and *I* show mosaic *mCerulean* reporter expression in the notochord at 24 hpf compared to  
213 gar element C which is not active in the zebrafish notochord (asterisk). N represent the number of animals  
214 expressing *mCerulean* in the notochord relative to the total number of animals expressing mosaic  
215 *ubi:mCherry* as injection control. Scale bar in B: 0.5 mm, applies to B-F.  
216 (E,F) Representative F0 zebrafish embryos injected with the conserved zebrafish enhancer elements *dr\_T3*  
217 (E) and *dr\_I* (F). *T3* and *I* show mosaic *mCerulean* reporter expression in the notochord at 24 hpf. N represent  
218 the number of animals expressing *mCerulean* in the notochord relative to the total number of animals  
219 expressing mosaic *ubi:mCherry* as injection control.  
220 (G,H) Representative images of stable F1 embryos at 2 dpf of zebrafish enhancer elements *T3* and *I*  
221 recapitulate the F0 expression pattern in the notochord, with *dr\_T3* (E) additionally expressing *mCerulean* in  
222 the brain, heart, and fin, and *dr\_I* (G) in the proximal kidney close to the anal pore, pharyngeal arches, heart,  
223 fin, and spinal cord neurons. Scale bar in G: 0.5 mm, applies to G,H.  
224 (I) Phylogenetic representation of species investigated using the bridging approach with spotted gar and  
225 painted turtle as anchor species within ray-finned fish and tetrapod lineages. Arrows indicate informative  
226 phylogenetic comparisons to uncover conservation of enhancer elements *T3*, *I*, and *C*. The species  
227 silhouettes were adapted from the PhyloPic database ([www.phylopic.org](http://www.phylopic.org)).

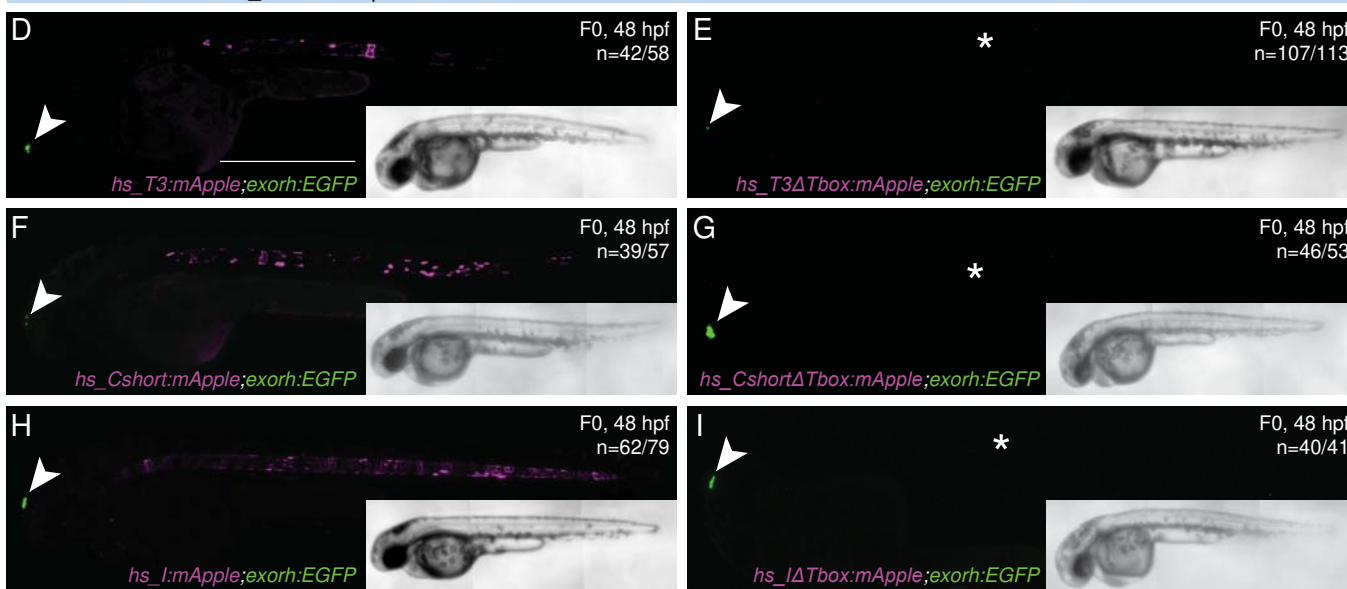
A



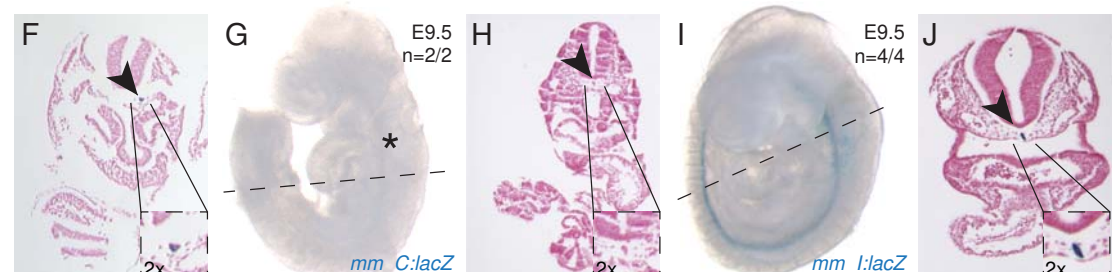
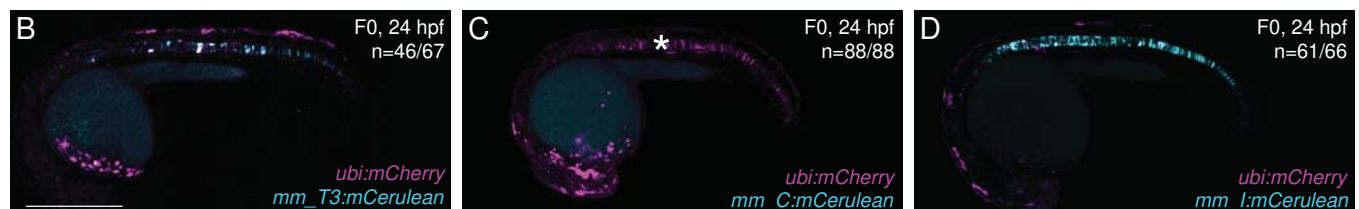
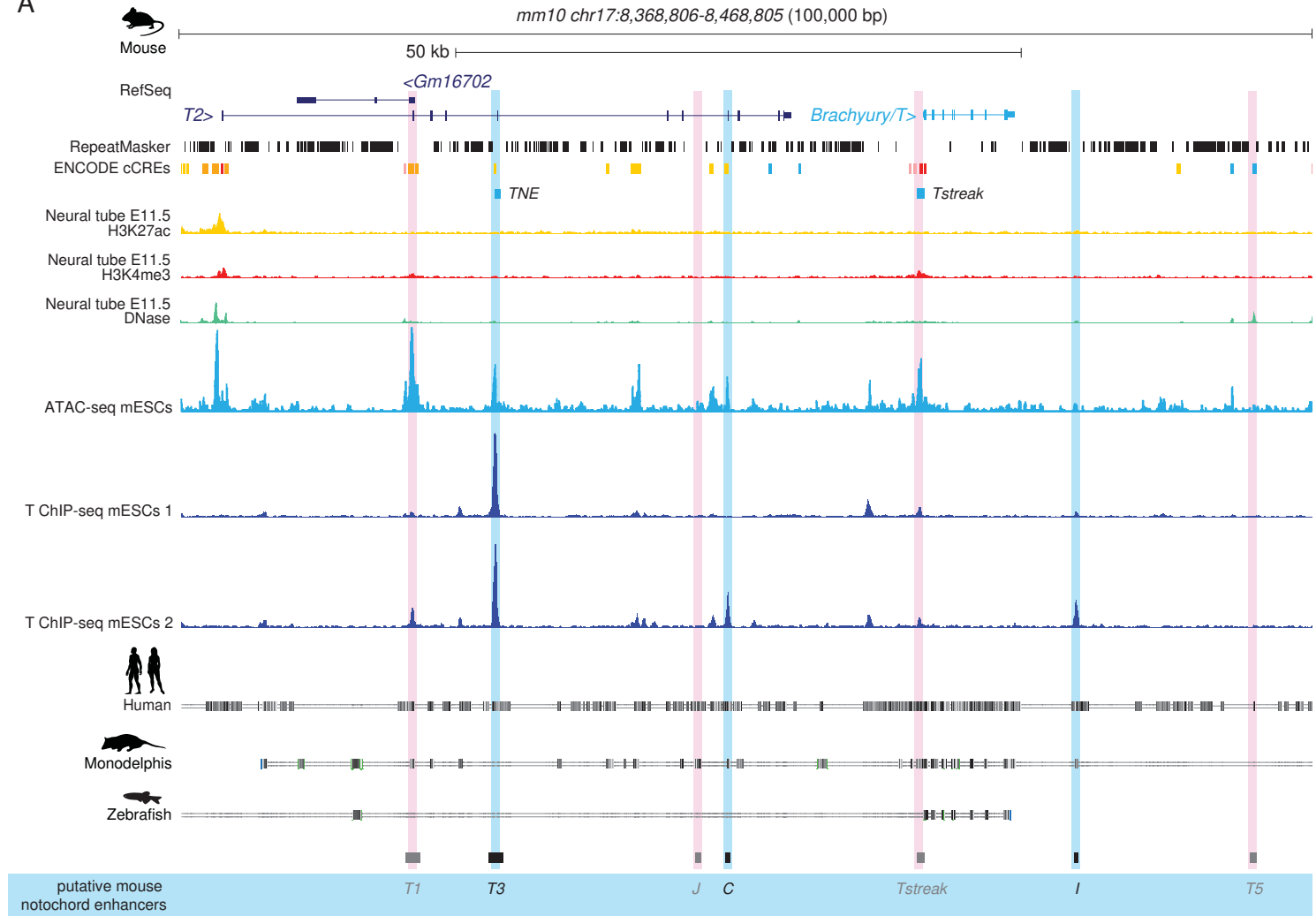


**B**

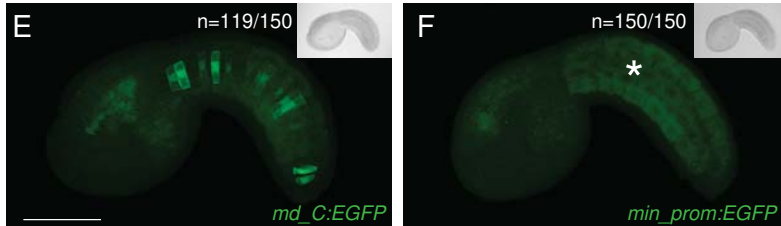
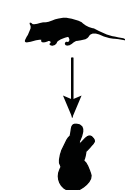
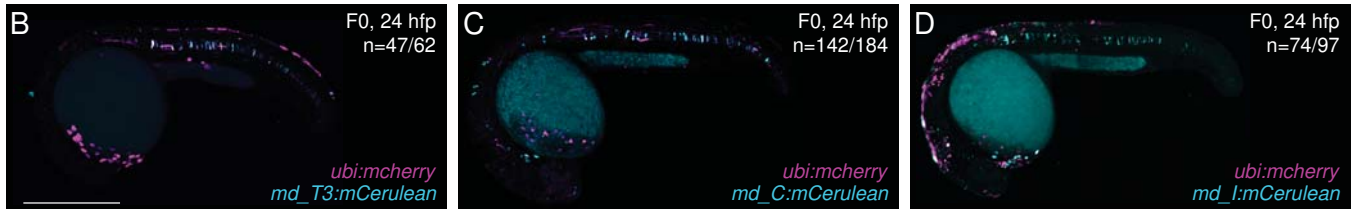
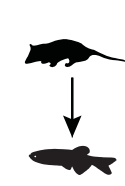
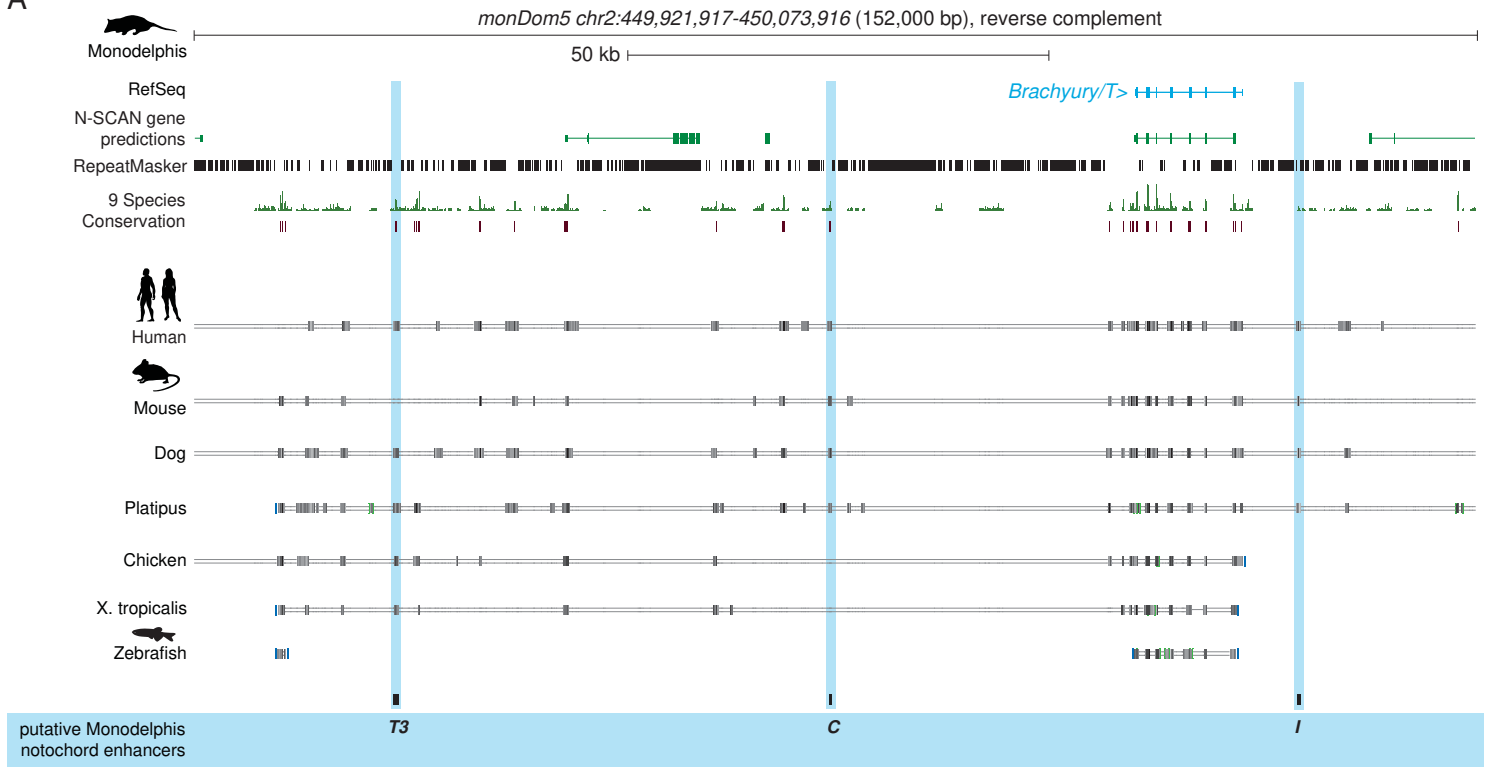
Motif ID	Name	Input	Length	Start	Stop	Strand	Score	P value	Q value	Matched sequence
MA0009.2	TBXT	<i>hs_T3</i>	409 bp	130	145	+	7.80769	0.00007	0.0323	CCTCACCTTTTGTGA
MA0009.2	TBXT	<i>hs_T3</i>	409 bp	130	145	-	8.38462	0.0000563	0.0312	TCACAAAAAGGTGAGG
MA0009.2	TBXT	<i>hs_T3</i>	409 bp	277	292	+	9.03846	0.0000438	0.0312	TCACAGTTGCTGTGA
MA0009.2	TBXT	<i>hs_T3</i>	409 bp	277	292	-	8.96154	0.0000451	0.0312	TCACAGCAAATGTGA
MA0009.2	TBXT	<i>hs_C</i>	415 bp	184	199	+	-7.88462	0.00473	1	CCGCAGTTGGCTGGGG
MA0009.2	TBXT	<i>hs_C</i>	415 bp	184	199	-	-7.82692	0.00468	1	CCCCAGCCAACGTGCGG
MA0009.2	TBXT	<i>hs_C</i>	415 bp	201	216	+	-9.55769	0.00648	1	TAGCACCAACAGAGA
MA0009.2	TBXT	<i>hs_C</i>	415 bp	201	216	-	-10.6923	0.00793	1	TCTCTGTTGGTGCTA
MA0009.2	TBXT	<i>hs_I</i>	604 bp	309	324	+	10.7692	0.0000216	0.0312	TCCCACATAGGTGAGG
MA0009.2	TBXT	<i>hs_I</i>	604 bp	309	324	-	9.57692	0.0000353	0.0312	CCTCACCTATGTGGGA



A



A



A

### *Brachyury/T>*

wildtype allele:

$T2 >$

double knock-out allele:  $T^{\Delta C, I}$

single knock-out allele:  $T^{\Delta}T3$

triple knock-out allele:  $T^{\Delta T3,C,I}$

## enhancer elements

ΔT3

1

### Brachyury levels in notochord

### wildtype

T  $\Delta C, I/\Delta$

$$T \Delta C_p / \Delta$$

---

 $T \Delta T 3/\Delta T 3$

### $T \Delta T3/\Delta T3, C, I$

$\Delta T3, C, I / \Delta T3, C, I$

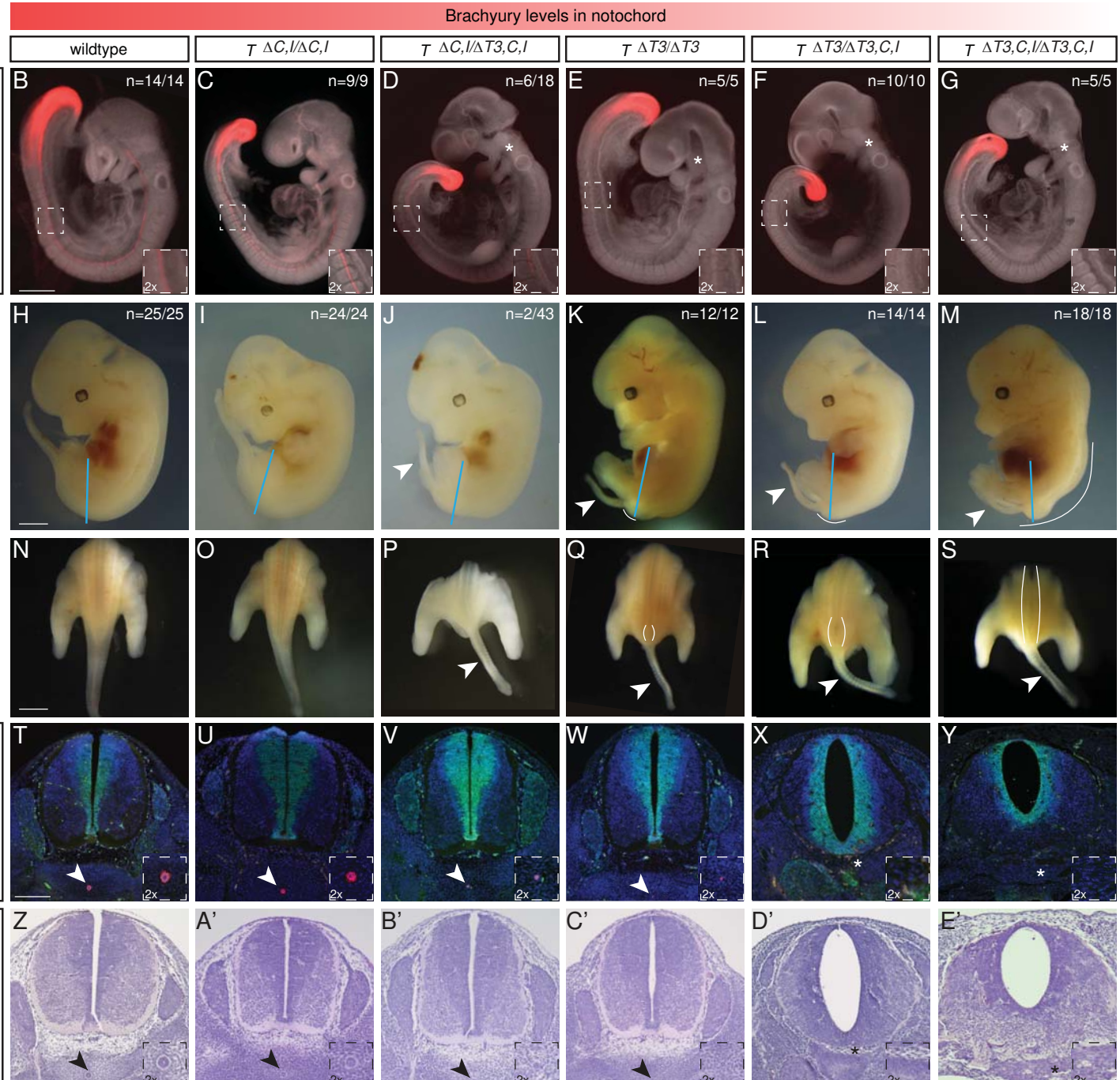
E9-9.5

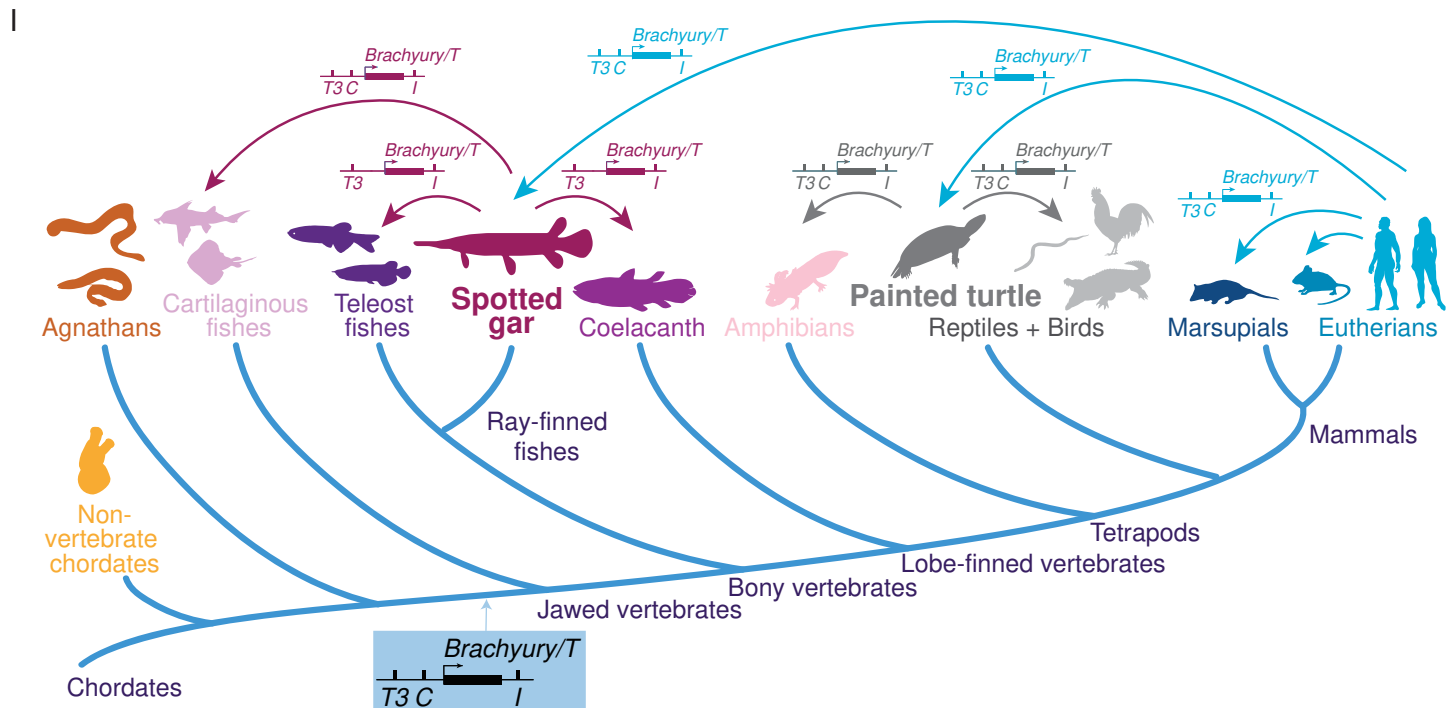
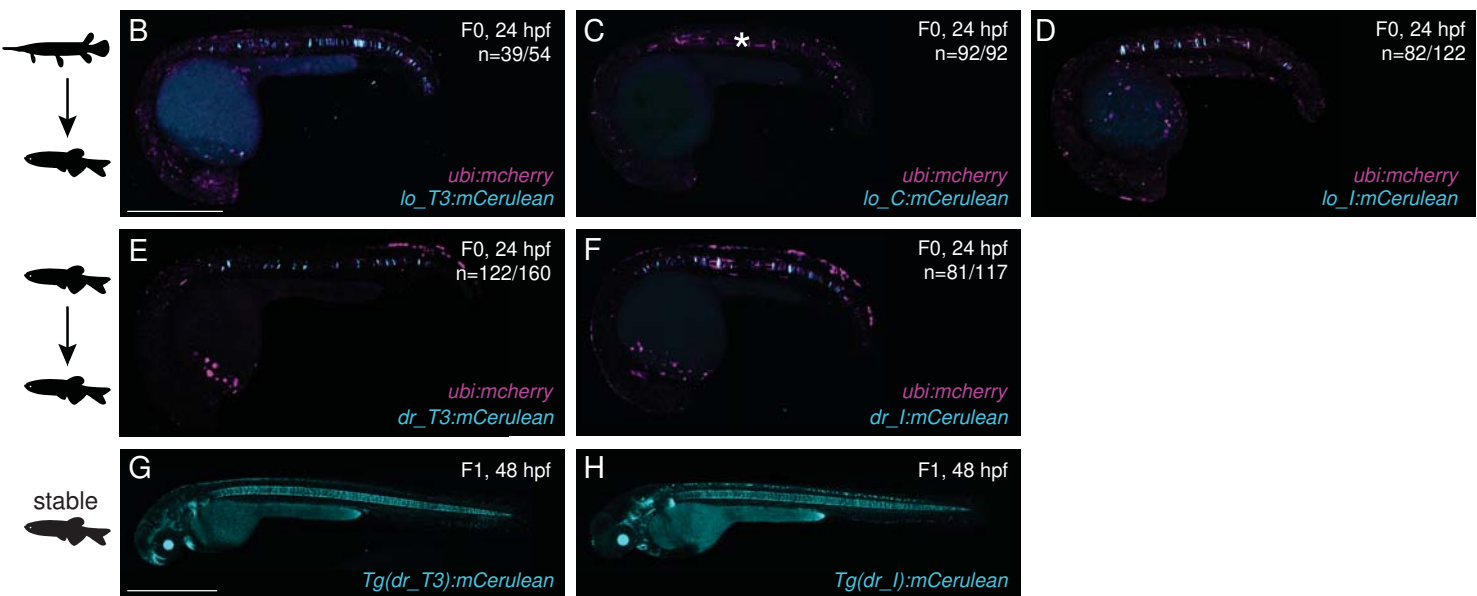
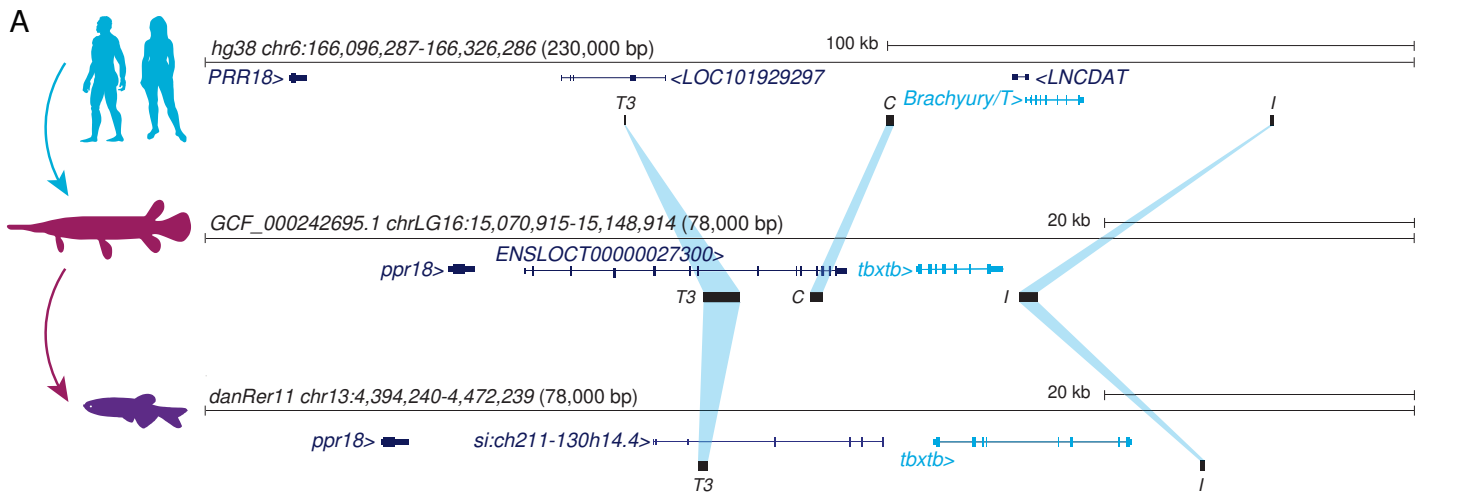
anti-Tbx1

12.5

anti-Tbx1 DAP

H&E anti-So





**Supplementary Information to the manuscript: Conserved enhancers control notochord expression of vertebrate Brachyury by Kemmler et al.**

**This Supplementary Information contains information about the Supplementary Data 1-7, as well as Supplementary Figures 1-6. Supplementary Data 1-6 are excel tables, Supplementary Data 7 are MAFFT alignments and sequence files compiled as a .zip file.**

**Supplementary Data 1: Genomic features of the human enhancer elements.**

Summary table listing the genomic features of the human enhancer elements, including length, location relative to transcription start (TS) site, ATAC- or T ChIP-seq peaks, conservation in mouse and *Monodelphis*, H3K27ac, and ENCODE cCREs.

**Supplementary Data 2: Reporter activity across animal models.**

All numbers from the enhancer reporter experiments in zebrafish, axolotl, mouse, and Ciona.

**Supplementary Data 3: Coordinates of all cloned enhancer elements.**

Summary table displaying the genomic coordinates of all enhancer elements from different species, as well as primer sequences used to amplify them, length, and reporter activity of the enhancers in the different species.

**Supplementary Data 4: *Tbx3b* enhancer element conservation across vertebrates.**

Genomic location and genome versions are provided for each species. BLAST bridging chain is indicated with -> showing BLAST hits from *Tbx3b* loci of one species to another and -x indicating lack chaining. (2x) indicate tetraploid species with up to two *tbx3b* loci.

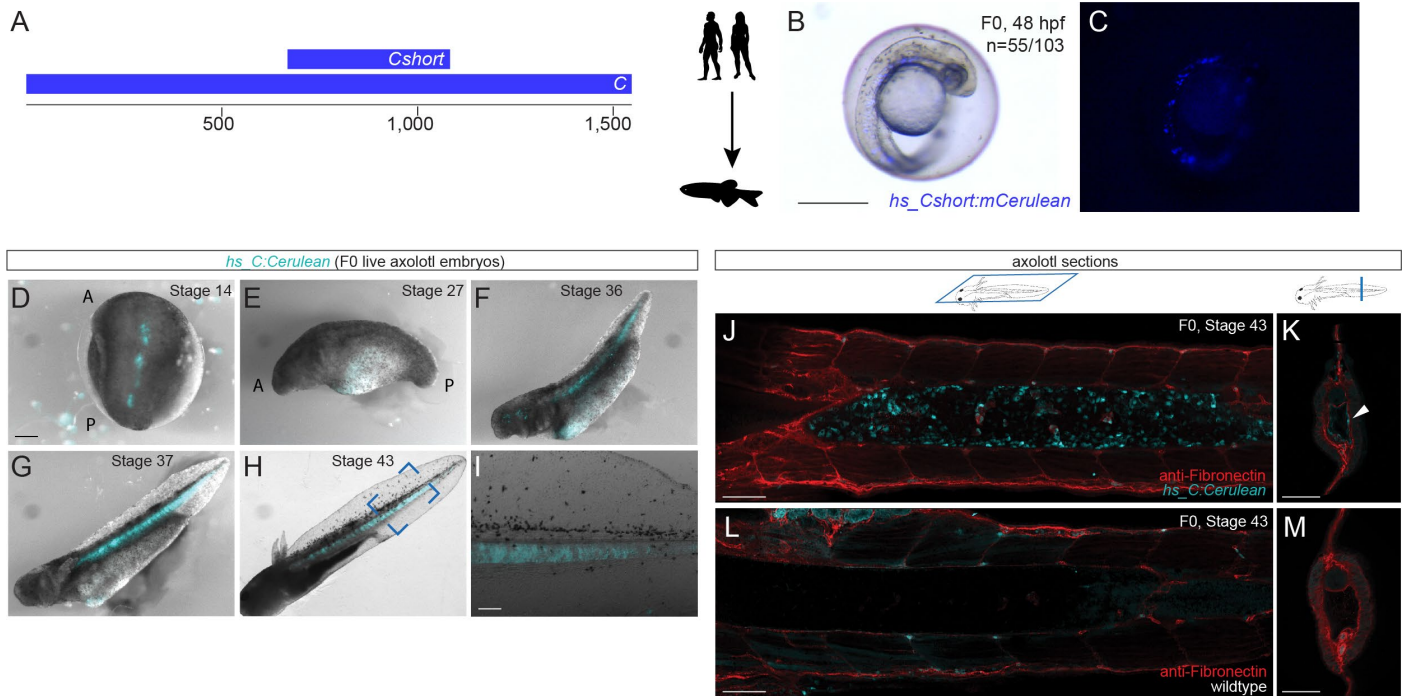
**Supplementary Data 5: Enhancer element deletions and primer sequences for genotyping.**

Summary table with genomic coordinates and sequences of the used target sites, primer, and sequences of the three enhancer deletions.

**Supplementary Data 6: Qualitative evaluation of Brachyury antibody staining in E9.5 embryos.**

Summary table of qualitative evaluation of anti-Brachyury/T staining in E9.5 embryos.

**Supplementary Data 7: Sequence and alignment files of *T3*, *C*, and *I* for Fig. 6 and Supplementary Fig. 6**



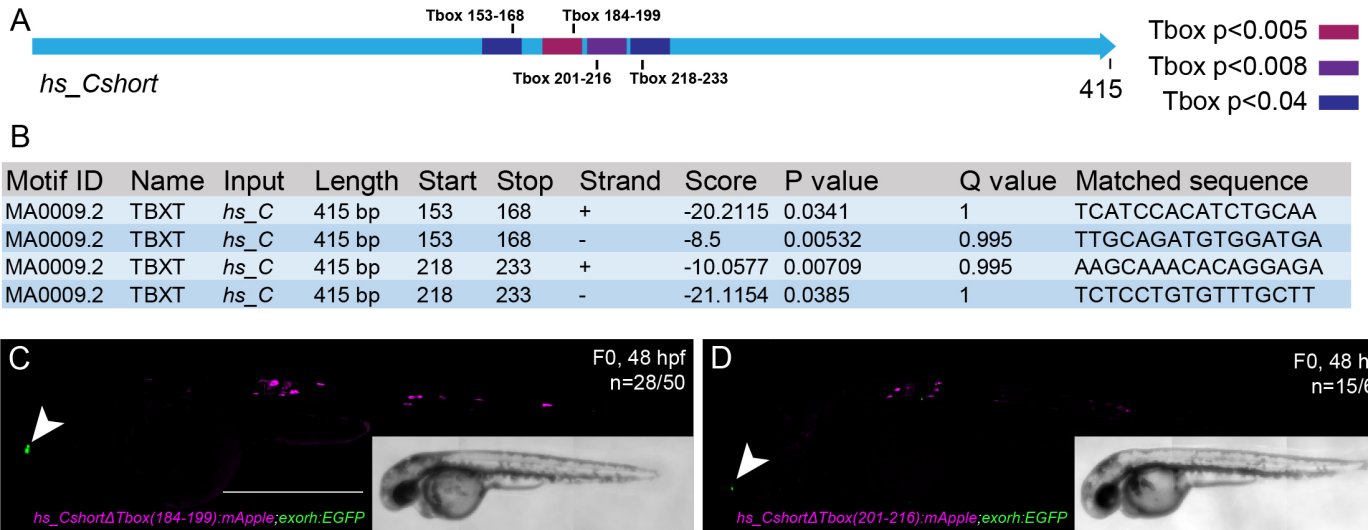
**Supplementary Figure 1: Human enhancer element *Cshort* in zebrafish and time course of human enhancer element *C* in axolotl.**

(A) Schematic representation of human enhancer element *C* and *Cshort*.

(B,C) Representative F0 transgenic zebrafish embryo expressing *hs\_Cshort:mCerulean* in the notochord at 2 dpf. Images shown are a merge of bright field and fluorescence (B) and fluorescence only (C). Scale bar in B: 0.5 mm, applies to B,C.

(D-I) Live images of representative F0 transgenic axolotl embryos expressing *hs\_C:mCerulean* at stages 14 (D), 27 (E), 36 (F), 37 (G), 43 (H) and close up of H from the blue outline (I). (D) dorsal view. (D,E) A, anterior, P, posterior. Images shown are a merge of bright field and fluorescence. Scale bar in D: 1 mm; applies to panels D-H. Scale bar in I: 0.5 mm.

(J-M) Confocal images of horizontal (J,L) and cross (K,M) sections through the axolotl embryo (stage 43) show mCerulean fluorescence in the notochord in transgenic *hs\_C:mCerulean* embryos (J,K) compared to wildtype embryos (L,M), but not in the surrounding muscle which is highlighted by immunostaining of fibronectin in red. Scale bars in J-M: 0.5 mm. The species silhouettes were adapted from the PhyloPic database ([www.phylopic.org](http://www.phylopic.org)).

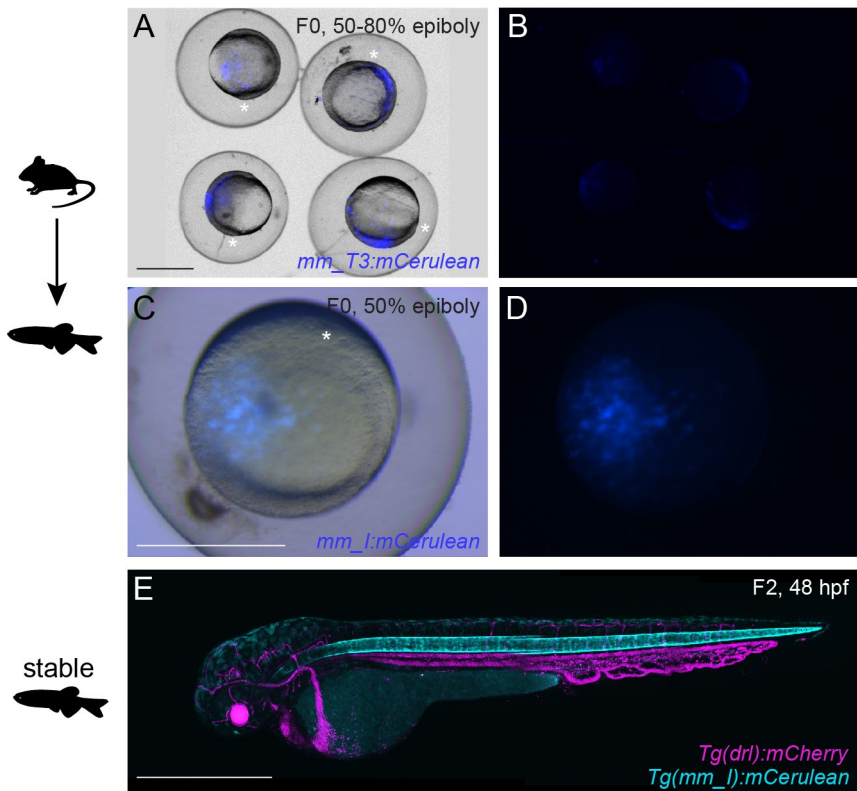


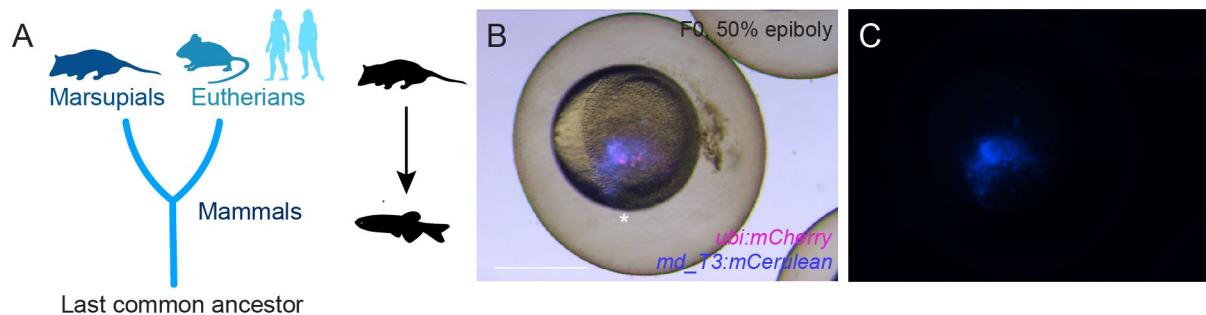
### Supplementary Figure 2: Additional identified TBXT binding sites in enhancer C.

**(A)** Schematic depiction of the human enhancer element *hs\_Cshort* including the four TBXT binding sites/T-box motifs with different p-values; reverse complement direction. P values were calculated by FIMO.

**(B)** FIMO output with location of the T-box motifs, statistical significance, and matched sequence within the enhancer elements.

**(C,D)** Injection of the enhancer element *hs\_Cshort* with individual deleted T-box motifs *hs\_CshortΔTbox(184-199)* **(C)** and *hs\_CshortΔTbox(201-216)* **(D)** as reporter constructs results in maintained reporter activity. Arrowheads **(C,D)** mark EGFP expression in the pineal gland from the transgenesis marker *exorh:EGFP*. Scale bar in **C**: 0.5 mm, applies to **C,D**.

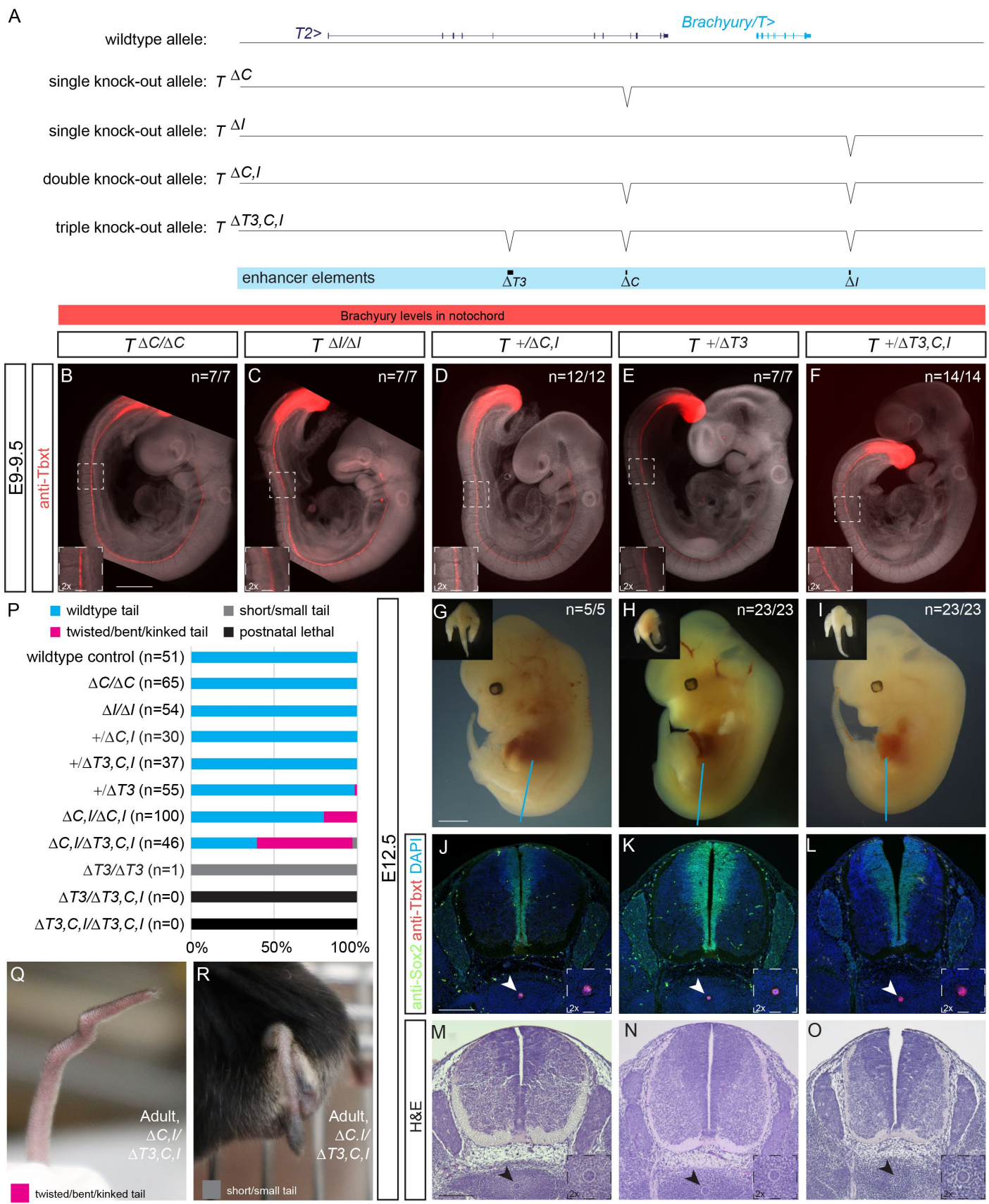




**Supplementary Figure 4: Additional data to *Monodelphis domestica* enhancer elements.**

**(A)** Mammalian phylogeny outlining the split into Marsupials and Eutherians.

**(B,C)** *Monodelphis* enhancer element *md\_T3* in zebrafish at 80% epiboly. Live images of representative F0 transgenic zebrafish embryos expressing *md\_T3:mCerulean* and *ubi:mCherry* in the zebrafish embryo at 80% epiboly. Images shown are a merge of bright field and fluorescence (**B**) and fluorescence only (**C**). Scale bar in **B**: 0.5 mm, applies to **C**. Asterisk in **B** marks the shield. The species silhouettes were adapted from the PhyloPic database ([www.phylopic.org](http://www.phylopic.org)).



**Supplementary Figure 5: Additional data to deletion of the three enhancer elements.**

**(A) Mouse *Brachyury/T/TBX5B* locus adapted from UCSC browser and annotation of single knockout alleles *AC* and *AI*.**

**(B-F)** E9.5 homozygous  $\Delta C$  (**B**), homozygous  $\Delta l$  embryos (**C**), heterozygous  $+\Delta C, l$  (**D**), heterozygous  $+\Delta T3$  (**E**), and heterozygous  $+\Delta T3, C, l$  embryos (**F**) display normal Brachyury/T protein expression (red) in the notochord as depicted by anti-T immunofluorescence. White dashed square in panels represents location of right bottom inserts with 2x magnification. Scale bar in **B**: 1 mm, applies to panels **B-F**

**(G-I)** Overall morphology of E12.5 embryos with different genotypes. Inserts in the left upper corner represent

anterior view of the trunk and tails. Blue lines indicate the location of immunofluorescence and H&E sections. Inserts in the top left indicate wildtype looking tails. Scale bar in **G**: 1 mm, applies to panels **G-I**.

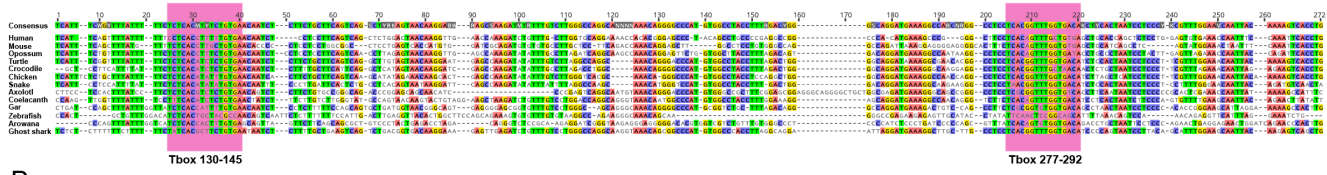
**(J-L)** Immunofluorescence of mouse transverse sections. Anti-Sox2 labels the neural plate, anti-Tbx5 the notochord, and DAPI marks nuclei. Sox2 and Brachyury/T expression is comparable amongst the shown genotypes. Scale bar in **J**: 0.2 mm, applies to **J-L**.

**(M-O)** H&E staining of transverse sections confirm normal notochords. Arrowheads point to notochord. Scale bar in **M**: 0.2 mm, applies to **M-O**.

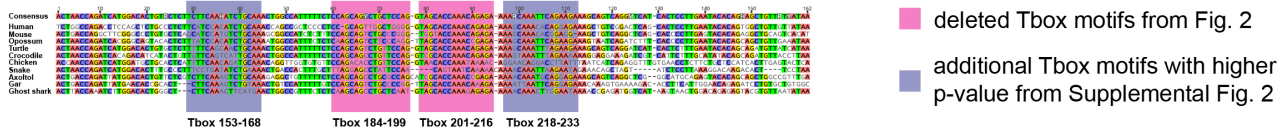
**(P)** Percentage of adult animals with tail phenotypes.

**(Q,R)** Representative images of the kinked and small tail phenotype in  $T^{\Delta C, /} / \Delta T3, C, /$  trans-heterozygous adult animals.

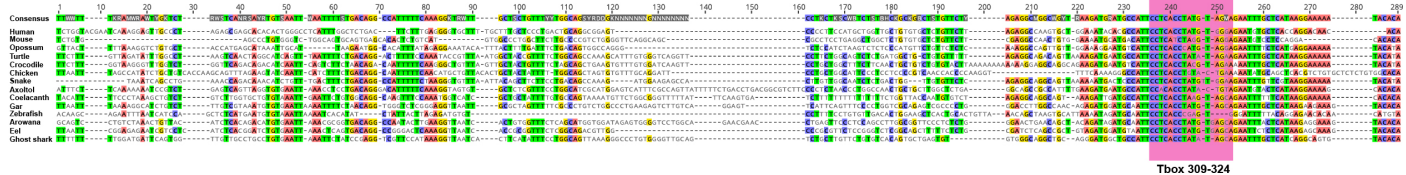
### A *hs\_T3*



### B *hs\_C*



### C *hs\_I*



**Supplementary Figure 6: Conservation of the enhancers *T3*, *C*, and *I* with their respective T-boxes.**  
**(A-C)** Conservation of the enhancers *T3* (A), *C* (B), and *I* (C) and respective T-box motifs in different species. T-box motifs with low p-value are marked in pink (see Fig. 2) and T-box motifs with higher p-value are marked in violet (see Supplementary Fig. 2).

**Supplementary Data 1: Genomic features of the human enhancer elements.**

Summary table listing the genomic features of the human enhancer elements, including length, location relative to transcription start (TS) site, ATAC- or T ChIP-seq peaks, conservation in mouse and *Monodelphis*, H3K27ac, and ENCODE cCREs.

**Supplementary Data 2: Reporter activity across animal models.**

All numbers from the enhancer reporter experiments in zebrafish, axolotl, mouse, and Ciona.

**Supplementary Data 3: Coordinates of all cloned enhancer elements.**

Summary table displaying the genomic coordinates of all enhancer elements from different species, as well as primer sequences used to amplify them, length, and reporter activity of the enhancers in the different species.

**Supplementary Data 4: *Tbx1b* enhancer element conservation across vertebrates.**

Genomic location and genome versions are provided for each species. BLAST bridging chain is indicated with -> showing BLAST hits from *Tbx1b* loci of one species to another and -x indicating lack chaining. (2x) indicate tetraploid species with up to two *tbx1b* loci.

**Supplementary Data 5: Enhancer element deletions and primer sequences for genotyping.**

Summary table with genomic coordinates and sequences of the used target sites, primer, and sequences of the three enhancer deletions.

**Supplementary Data 6: Qualitative evaluation of Brachyury antibody staining in E9.5 embryos.**

Summary table of qualitative evaluation of anti-Brachyury/T staining in E9.5 embryos.

**Supplementary Data 7: Sequence and alignment files of *T3*, *C*, and *I* for Fig. 6 and Supplementary Fig. 6**